An *in vitro* neurogenetics platform for precision disease modeling in the mouse

Daniel E. Cortes, Mélanie Escudero, Arojit Mitra, Austin C. Korgan, Alyssa Edwards, Selcan C. Aydin, Steven C. Munger, Zhong-Wei Zhang, Kristen M.S. O'Connell, Laura G. Reinholdt, and Martin F. Pera[1]

The Jackson Laboratory Bar Harbor ME 04660 USA

[1] Author for correspondence martin.pera@jax.org

Keywords: mouse and human pluripotent stem cells, precision disease modeling, neurodevelopment, neurogenetics, *DYRK1A*, neuronal repair

Summary

The mouse is often the model of choice for genetic analysis of neurological disorders, but the introduction of pathogenic mutations into a single inbred strain sometimes fails to yield phenotypes relevant to human disease. Interrogating genetically diverse panels of mice can identify better models of human sensitivity and resistance to candidate disease variants. We developed an *in vitro* methodology for modeling multiple stages of central nervous system development using a panel of genetically diverse mouse embryonic stem cell lines. Chemical knockdown of the neurodevelopmental gene *Dyrk1a* demonstrated profound strain differences in the cellular response to the ablation of DYRK1A activity throughout development *in vitro*. Responsive strains showed *in vitro* developmental defects consistent with those observed *in vivo* in *Dyrk1a* knockout mice, and mirrored the phenotype seen in neural progenitors derived from *DYRK1A* knockout human pluripotent cells. Transcriptomic analysis of differentiated cells from sensitive and resistant cell strain backgrounds successfully identified key molecular pathways in neural development known to be associated with *Dyrk1a* haploinsufficiency *in vivo*. Thus, comparative phenotypic analysis of differentiated cells from human and genetically diverse mouse pluripotent stem cells bearing disease mutations provides a facile route to identification of optimal mouse strains for precision disease modeling *in vivo*.

Introduction

Experimental platforms based on human pluripotent stem cells (hPSC), including two-dimensional cultures and three-dimensional organoid models of specific brain regions, are playing an increasing role in the study of the development of the central nervous system, and in unraveling the genetics of brain disorders (Fernando et al., 2020). However, most neurologic or psychiatric disorders are highly complex, involving the interaction of multiple systems inside and outside of the central nervous system (CNS). The laboratory mouse has provided a versatile and practical model for the study of CNS disorders. The mouse has homologues of most human genes and is amenable to facile genetic manipulation, and well-established methodologies for phenotyping at the levels of electrophysiology, imaging, cognition, and behavior are available in the species.

Most mouse models for heritable human disorders have been created in a few commonly used inbred strains. However, genetic background can have profound effects on the phenotype of a particular mouse model. Thus, creating a gene knockout or mutation model on a single genetic background may or may not yield a phenotype relevant to human disease. This impediment to disease modeling has long been apparent from studies of mouse knockouts on different genetic backgrounds (Chandler et al., 2013; Erickson, 1996), and can generally be related to the effects of modifier genes (Riordan and Nadeau, 2017). To a considerable degree, incorporating greater genetic diversity into disease modeling in the mouse can provide a more reliable reflection of human disease pathogenesis than studies with a few inbred strains. A number of recent reports have shown clearly how the use of genetically diverse strain backgrounds can enhance our ability to model human sensitivity and resilience to disease, as exemplified in studies of Alzheimer's Disease, Type 2 diabetes, autism and gastric cancer (Keller et al., 2018; Li and Auwerx, 2020; Molenhuis et al., 2018; Moore et al., 2020; Neuner et al., 2019; Onos et al., 2019; Sittig et al., 2016; Swanzey et al., 2021). However, the establishment, maintenance and use of mouse diversity panels requires significant infrastructure, animal husbandry, and genetics resources, limiting their implementation for many investigators.

In recent years, mouse embryonic stem cell (mESC) lines from genetically diverse mouse strains have become available, and they have been used *in vitro* to study the genetic basis of the permissiveness of strains for mESC establishment, the regulation of the pluripotent state and early lineage specification, and the stability of genomic imprinting *in vitro* (Czechanski et al., 2014; Garbutt et al., 2018; Onos et al., 2019; Ortmann et al., 2020; Sittig et al., 2016; Skelly et al., 2020; Swanzey et al., 2020; Swanzey et al., 2021). Here we report a novel paradigm for the application of genetically diverse mESC lines to *in vitro* disease modeling in the CNS, a precision neurogenetics approach that has the potential to make mouse genetic diversity more accessible to the research community, and to provide for facile selection of appropriate mouse genetic backgrounds for human disease modeling. We previously established a set of robust neural differentiation protocols that enable production of key CNS cells of interest from genetically diverse inbred strains and even hPSC (Cortes et al. unpublished). These protocols are applicable across a panel of mESC representative of wide genetic diversity, encompass multiple

stages of neural development, and provide for functional readouts. Using high content screening, RNA-seq, electrophysiology, axonal regeneration paradigms, and knockout models, we provide here a proof-of-concept study in the form of a chemogenomic analysis of the effects of inhibition of the neurodevelopmental gene, dual-specificity tyrosine phosphorylation-regulated kinase 1A (*Dyrk1a),* at multiple stages of neurogenesis and axonal repair. *Dyrk1a* was first discovered in Drosophila and the gene named “minibrain” because mutations in the gene causes size reduction of the optic lobes and central brain hemispheres (Tejedor et al., 1995). *Dyrk1a* gene dosage affects many stages of neural development. In human, *DYRK1A* is located on Chromosome 21 and it has been associated with a range of conditions including Alzheimer's Disease, Down syndrome, microcephaly, autism, and intellectual disability, (Arbones et al., 2019; Branca et al., 2017; Dang et al., 2018; Earl et al., 2017; Feki and Hibaoui, 2018; Fernandez-Martinez et al., 2015). Interestingly, patients harboring the same point mutation in the *DYRK1A* gene display different phenotypes ranging from severe autism to relatively minor neurological impairment (Earl et al., 2017), strongly suggesting that the genetic background modifies the penetrance of the mutation.

Using genetically diverse mESC, we demonstrate the impact of genetic background on the outcome of DYRK1A inhibition across multiple stages of neural development. With this approach, matching *in vitro* phenotypes in hPSC-based disease models with mESC models exhibiting similar sensitivity or resilience to pathogenic mutationsenables rapid selection of mouse genetic backgrounds for *in vivo* modeling studies, and will provide a platform for prospective analysis of the power of *in vitro* mutant phenotyping to predict disease phenotype *in vivo,* a critical component of functional genomics analysis going forward.

Results

Our overall objective was to develop in vitro methodology for the assessment of the effects of genetic variants on neural development and disease across eight highly genetically diverse mESC representing the founders of the Collaborative Cross (CC founders, A/J (AJ), C57BL/6J (B6), 129S1/SvImJ (129), NOD/LtJ (NOD), NZOHiLtJ (NZO), CAST/EiJ (CAST), PWD/PhJ (PWD), WSB/EiJ (WSB)). For a proof-of-concept study, we decided to examine how genetic background impacts on the effect of DYRK1A inhibition during neuronal development at different stages. *Dyrk1a* also regulates axonal growth and guidance, so we decided to assess an experimental model of axon regrowth as well (Figure 1). We used the well-characterized DYRK1A inhibitor ID-8; this inhibitor is highly selective against DYRK1A compared to other kinases. ID-8 IC_{50} values for DYRK1A, GSK3b, and CLK1 are 78, 450, and 4200 nM respectively, and DYRK2, DYRK3, and DYRK4 are not affected at all (Bellmaine et al., 2017; Hasegawa et al., 2012; Miyabayashi et al., 2008; Monteiro et al., 2018). To ascertain that differences in phenotypes are not merely a consequence of differences in gene coding sequences or expression levels across the strains, we examined both. We first looked for SNPs and number of transcriptional isoforms. We found that CAST and PWD/K were more divergent than the reference genome (B6) while the other strains were closely related (Figure 2A). It is worth noting however that the divergence in the genotypes, even for CAST and PWD/K do not affect the protein sequence, suggesting that catalytic activity remains unaltered and nucleotide mutations on all exons are synonymous (Table S1). Examination of expression quantitative trait loci (eQTL), in both mESC (Aydin et al., 2023; Skelly et al., 2020) and NPCs (Aydin et al., unpublished) revealed a local eQTL in CAST and PWD/K suggesting a diminished expression of *Dyrk1a* mRNA in those two cell lines (Figure 2B). Nevertheless, we could not find any protein QTL among all the strains, indicating that despite the differences in genotype and eQTL in CAST and PWD/K, no differences in expression at the protein level were anticipated (Figure 2C). We measured protein levels in mESC from the eight mESC strains and found that although there is a slight decrease of DYRK1A protein in CAST, NOD, and PWD, these differences were not statistically significant (Figure 2D & E). Overall, this shows that effects observed in the phenotype described below cannot be accounted for by strain differences in the coding sequence of *Dyrk1a* or its expression levels.

Effects of DYRK1A inhibition on mESC maintenance and lineage specification vary across genetically diverse mouse strains.

It was previously shown that DYRK1A inhibition by ID-8 in mESC and hPSC helps to maintain the pluripotent state, and that either chemical inhibition or knockdown hampers specification from the pluripotent state to the neural lineage in hPSC (Bellmaine et al., 2017; Miyabayashi et al., 2008). In order to study pluripotency maintenance and lineage biases across mESC from different strains to compare with previous work on 129 mESC and hPSC, we cultured the eight mESC lines in media supplemented with four combinations of factors: LIF+2i (LIF plus PD0325901 and CHIR99021,optimal maintenance of naïve state mESC, (Ying et al., 2008)), LIF+ID-8, LIF, and ID-8. These

cell lines were previously shown to vary in their response to LIF and in the stability of the undifferentiated state (Nichols et al., 2009; Skelly et al., 2020); some lines remain in the undifferentiated state and others switch on lineage markers as soon as LIF+2i optimal conditions are abandoned, especially those mESC lines from strains regarded to be recalcitrant to stem cell derivation (Czechanski et al., 2014).

Using high content screening (HCS), we analyzed the expression of ten different pluripotency and lineage specific markers during four days of culture in the above conditions (Figure 3A, B, Figure S1). Only LIF+2i was able to maintain the expression of the pluripotency associated factors POU5F1, NANOG and SOX2 in all cell lines; nonetheless, PWD and NZO expressed these markers at low levels under all conditions. ID-8 was originally found to substitute for LIF in mESC maintenance on the 129 background (Miyabayashi et al., 2008). Comparing cultures grown in LIF+2i with ID-8, we note that 129, AJ and B6 show the best maintenance of NANOG expression in ID8 alone (Figure 3B, bottom panel). We also examined the proportion of cells expressing markers of the three embryonic germ layers (Figure 3B, top two panels). Those cell lines that showed consistent expression of pluripotency markers in ID-8 also showed low expression of most germ layer lineage markers. Colony morphometry using HCS provides another indicator of cellular response to the culture environment. Loss of stem cell marker expression generally correlated with changes in colony morphology, as morphometry showed that cell colonies became less compact and circular in ID-8 alone, and LIF+ID-8 enhanced roundness in 129 only (Figure 3C). Comparing LIF vs. ID-8 alone, the two conditions maintain pluripotency associated markers to a similar degree, but in 129, B6 and CAST, mesodermal markers are expressed at higher levels (Figure 3B, D). In summary these results confirm previous studies in 129 mESC and hPSC indicating that DYRK1A inhibition can help maintain the undifferentiated state. AJ and B6 derived mESC respond to ID-8 similarly to 129, but strains that are poorly maintained in LIF+2i are not rescued by DYRK1A inhibition.

DYRK1A inhibition differentially blocks neural progenitor proliferation in a strain-dependent fashion

Next, we used our differentiation system to study multiple stages in neural development, from neural lineage specification through to neurogenesis, neuronal differentiation, and maturation. For this, we differentiated the eight mESC lines into NPCs using our newly developed protocol in the absence or presence of ID-8, and analyzed the cultures at the beginning and on days two, five, and eight via immunostaining and HCS (Figure 4A-B). As noted above, all pluripotency-associated markers were highly expressed at Day 0. After two days of differentiation, lineage markers for all three germ layers were detectable while pluripotency associated markers were reduced (Figure 4A, top panel, and Figure S2). At day five of differentiation, pluripotency-associated markers, apart from POU5F1, were significantly reduced. By the endpoint of differentiation (day eight), cells had a fully developed neural morphology, with characteristic rosettes and neurites emerging from the cell clusters (Figure 4A, mid and bottom panels). All cell lines showed robust

expression of neural lineage markers, with continued cell proliferation, and low expression of mesoderm and endoderm markers (Figure S2).

Following induction of neural specification in the presence of ID-8, B6 cultures contained lower percentages of OTX2 and TUBB3 positive cells, and displayed a marked reduction in the proportion of KI67 positive cells compared to control. Inhibition of the proliferation of neural progenitor cells during development is a hallmark of *Dyrk1a* haploinsufficiency. Further examination of the proliferation of neural progenitors from additional mESC clones of B6, AJ, 129 and WSB using KI67 and MCM2 immunostaining confirmed that the proliferation of B6 cells was strongly inhibited by ID8, whereas the latter three strains were unaffected (Figure 4C & D).

We previously observed an inhibition of neural specification in hPSC similar to that noted here (Bellmaine et al., 2017). We therefore examined the effect of heterozygous loss of *DYRK1A* on neural progenitor proliferation in the human induced pluripotent stem cell (hiPSC) line KOLF2.1J (Pantazis et al., 2022). The susceptibility of B6 neural progenitor cells to inhibition of proliferation by ID-8 was mirrored in the reduced growth of *DYRK1A*+/- human iPSC neural progenitors relative to controls (Figure 4E). Thus, in terms of effects of DYRK1A inhibition on the maintenance of the undifferentiated state, interference with neural specification, and reduction of neural progenitor proliferation, the B6 mESC display the best face validity for modeling the response of human pluripotent stem cells to DYRK1A inhibition or haploinsufficiency.

To corroborate that the observed neural differentiation impairment is caused by ID-8-induced DYRK1A inhibition; we generated *Dyrk1a* knock-out mESC lines, specifically on B6, 129 and WSB backgrounds. We conducted NPC differentiation on these cell lines and analyzed the phenotype. Similar to results with chemical knockdown of DYRK1A, we observed that the only strain severely affected by *Dyrk1a* KO was B6, whilst neural progenitor specification, proliferation and differentiation in WSB and 129 cell lines were indistinguishable from parental controls. During B6 knockout cell line differentiation, we observed a decreased expression of proliferation and neural markers, and a decreased number of cells (Figure S3).

Although all strains had different degrees of response to ID-8 during neural progenitor specification and expansion, WSB was the most unresponsive while B6 was the most affected. Bulk RNA-seq was performed on these two cell lines at day eight of differentiation to identify the differences in gene expression associated with the extreme phenotypic differences found between WSB and B6. This difference in response to the inhibitor is evident from the numbers of differentially expressed genes (DEG); there were more than 700 DEG between B6 control and ID-8 treated cultures, but only 13 for control or treated WSB (Figure 5A). In control conditions, the expression profile of cells from both strains was substantially different, and this pattern was accentuated after treatment; from 189 DEG to more than 1400 (Figure 5A).

Regulatory transcriptional network analysis (RTNA) revealed *Foxb1*, *Hoxa4*, and *Hoxd3* as the top regulons associated with the differences found between WSB and B6 in

response to ID-8 treatment (Figure 5B). *Foxb1* is a regulator of neural progenitor differentiation (Zhang et al., 2017), and is rapidly and transiently induced during cortical specification of hPSC (van de Leemput et al., 2014). The two Hox genes are associated with hindbrain patterning in the CNS (Alexander et al., 2009).

Gene ontology (GO) analysis indicated that either under control conditions or in the presence of ID-8, DEG associated with the response to LIF were highly overrepresented in B6 vs. WSB (Figure 5C, upper panel). The LIF signaling pathway is responsible not only for maintenance of mESC but also for maintenance of mouse neural stem cells *in vitro* and i*n vivo* (Shimazaki et al., 2001). In the presence of ID-8, DEG associated with the GO term synaptic membrane were overrepresented in WSB relative to B6 (Figure 5C lower panel), consistent with progression of neural differentiation in the former but not the latter.

Using the RNA-seq data, we also analyzed gene isoform changes due to treatment and between B6 and WSB strains. Isoform usage can change considerably even when there is no overall change in gene expression, with functional consequences (Desai et al., 2014), and *Dyrk1a* is known to regulate the activity of a number of RNA splicing proteins (Alvarez et al., 2003; Ding et al., 2012; Shi et al., 2008; Toiber et al., 2010). Global analysis showed that adding ID-8 induced a loss of exons in B6 strain but not in WSB. We found 200 unique genes with alternative isoform usage when control B6 cells were compared to WSB cells; an increase of variant isoforms between the two strains was observed in the presence of ID-8. Of particular interest was the finding that *Ntrk2* underwent a change in isoform expression in B6 NPC when treated with ID-8, whereas in WSB these isoforms remained unchanged (Figure 5D). *Ntrk2* codes for a neurotrophic receptor that binds BDNF. We found that ID-8 treatment induces a switch from the canonical isoform to an isoform lacking the kinase domain. This isoform is unable to transduce signaling via tyrosine phosphorylation, and it is notable that BDNF signaling was implicated in the response to *Dyrk1a* haploinsufficiency in a recent proteomics study in B6 mice (Levy et al., 2021).

These results suggest that, in the B6 strain in which neurogenesis is affected, DYRK1A inhibition interferes with multiple pathways involved in neural specification, patterning and differentiation. RNA-seq confirmed the resilience of WSB against, and susceptibility of B6 to, DYRK1A inhibition at the neural induction stage. Subsequent analysis highlighted key pathways in neurogenesis downstream of DYRK1A inhibition.

DYRK1A inhibition delays functional maturation of neurons and modulates gene expression of maturation-related genes in a strain dependent fashion

To understand how DYRK1A inhibition modulates physiological maturation of neurons, we used MEA plates capable of recording 16 field potentials per well on a 48-well plate to assess electrophysiological activity. We seeded young neurons and let them mature for six weeks while analyzing electrical activity at different time points (Figure 6A-B). Addition of ID-8 began two days after the NPCs were seeded and continued throughout.

All cell lines were capable of generating action potentials and bursts of spikes, and creating networks, but not all cell lines matured at the same rate. CAST, B6, and 129 were the cell lines that matured the fastest, measured by Hz, bursting activity, and synchrony, while PWD took the longest (Figure 6A-B). We found that in most of the strains, addition of ID-8 inhibited the development of electrical activity; neurons fired less and bursts of activity were less frequent. Complementarily, interburst intervals, the relative silent time between two trains of activity, were longer for most cell lines when ID-8 was added. Quantitative analysis of a range of parameters at the peak point of control electrical activity (Figure 6 B) confirmed inhibition of maturation across most strains by measurement of mean firing rate, number of bursts, prolongation of interburst intervals, and a reduction in spikes per burst. Two overall patterns were observed. In B6, CAST, A/J, and NOD, maturation was delayed and suppressed throughout the time course, whilst in PWD, 129, NZO, and WSB, maturation was delayed but activity recovered at the later time point (Figure 6B & C).

Taken together, once again the functional maturation of neurons from B6 mESC was sensitive to ID-8, that of WSB mESC-derived cells were partially resistant to ID-8, and NZO derived neurons were the most resilient among all the strains. A decreased rate of functional network maturation is consistent with known effects of ID-8 on axonal growth and dendrite arborization.

We next performed RNA-seq on WSB and B6 neurons. Analysis at this stage showed a similar pattern to the NPC stage on the MDS plot which separates the neurons by strain and treatment; it also showed more distance between B6 subgroups than the WSB counterpart indicating B6 was more affected by DYRK1A inhibition (Figure S4A). After ID-8 treatment, there were 220 DEG between WSB and B6 (Figure S4B). GO analysis of DEG differentially affected by ID-8 in the two strains identified biological adhesion and transmembrane receptor signaling, with WSB showing a greater enrichment following ID-8 treatment (Figure S4C). Cellular adhesion molecules are important for neural development and axonal growth (Togashi et al., 2009). *Rxrg*, *Dmrtb1*, and *Irf7* were the top regulons associated with the differences in response to DYRK1A inhibition between WSB and B6 neurons (Figure S4D). *Rxrg* has been associated with neurodegeneration (Majer et al., 2019) and *Irf7* is a key mediator of the innate and adaptive immune responses (Ning et al., 2011) and positively regulates microglia polarization to the M2 state. We also found more alternative splicing events in B6 compared to WSB neurons when treated with ID-8 (Figure S3E). An exemplary gene that showed isoform changes was *Slit2,* which is associated with axonal guidance and cell migration, and arborization (Ozdinler and Erzurumlu, 2002). *Slit2* exhibited isoform switches when treated with ID-8 in B6 neurons (Figure S3F) not observed in WSB counterparts.

mESC strain differences in recovery from axonal injury in vitro reflect genetics of recovery from brain injury in vivo

There are marked strain differences in the ability of different mouse strains to respond to injury to the CNS (Cortes and Pera, 2021). Abundant evidence confirms that *Dyrk1a* plays a role during neurite sprouting in normal development, and that gene dosage alteration affects axonal growth and dendrite arborization (Dang et al., 2018), but it is not known whether these developmental roles of *Dyrk1a* might be recapitulated during axonal regeneration. As a further test of the predictive power of our *in vitro* system, we performed axotomy to analyze differences in axonal regrowth in neurons derived from mESC from CC founder strains.

We differentiated the mESC into neurons and cultured them into microfluidic chambers. (Figure 7A). On these devices, neurons were seeded on one chamber and axons could traverse microgrooves reaching into a second chamber whereas somas could not. After four days, axons grew through to the second chamber (Figure 7B). However, the number of axons growing through to the second chamber, and their length and density, indicated by the total area occupied by axons, varied amongst mESC strains (Figure 7C). At this point, axons were cut off and left to recover for four more days while treated or untreated with ID-8. In all cases, under control conditions, more axons grew across the device and had longer processes than before injury, except for B6 neurons (Figure 7B-D). CAST, NOD and NZO grew significantly more following injury compared to all other strains. When ID-8 was added, most of the lines showed less growth than controls. WSB, AJ, and PWD axons occupied the same area after regrowth in the presence of ID8 as the control did (Figure 7D). WSB axons experienced the longest growth pre- and post-injury (both control and ID-8 treated). Notably, the extent of axon growth prior to injury was not predictive of the extent of regrowth post injury (e.g. 129 versus NZO versus B6, Figure 7C).

Because of this divergent response to injury between B6 and WSB, we again undertook bulk RNA-seq analysis on these two cell lines to identify the underlying transcriptional differences. Interestingly, MDS analysis demonstrated vastly different responses between the two strains in the response to axotomy in the presence or absence of ID-8. As we saw from experiments in the maturation stage, ID-8 affected the transcriptome in both strains in control or axotomized cultures. However, when axons are severed, the B6 transcriptome showed limited change, irrespective of ID-8 treatment, whereas WSB transcriptome shifts markedly in response to axotomy in control and ID-8 treated cultures. The combination of ID-8 and axotomy displays an additive effect on the transcriptome in WSB, whereas in B6 this response is not observed, as axonal cut with or without ID-8 (“no drug”) elicits the same effect (Figure 7E).

When axons were cut, the two cell lines (B6 and WSB) expressed a core set of genes. These genes were *Map11*, *Ntsr1*, *Ccn5*, *Slc16a3* and, *Smtnl2* reflecting GO associated with GO terms cellular response to hypoxia and neuron projection, both being part of a successful neuronal reaction to injury (Figure 7F). Top regulons for the differences found between the cell lines when injured were Ascl1, Creb5, and Olig2 (Figure 7G). These

transcription factors are important for neuronal differentiation and myelination. *Ascl1* has been associated with a superior regenerative capacity in dorsal root ganglion neurons in CAST versus B6 *in vivo* (Lisi et al., 2017). This differential expression pattern only emerged between the two strains after axonal injury.

After axons were cut and treated with ID-8, more genes were differentially expressed in WSB than in B6 (two-fold). Top common DEG genes in both cell lines were *Padi2*, *Calcr*, *Itgb4*, *Ifitm1*, *Npy*, *Tnfrsf11b*, *C1ra* and *Pcolce*; all of them are associated with axonal growth and guidance. In WSB-derived ID-8 treated neurons, gene sets associated with cell adhesion and central nervous system myelination were upregulated compared to the B6 counterpart (Figure 7H) and were confirmed by the number of hits per GO. This profile can explain a more robust axonal growth after axonal damage in WSB neurons. Finally, RTNA showed that two of the top three regulons associated with the differences in recovery after axonal growth, *Olig2* and *Ascl1,* were similar to those identified in the axonal damage response in the absence of ID-8. These results suggest that *Olig2*, *Creb5*, and *Ascl1* are part of the core regulatory network for a fast axonal growth after axonal damage when B6 and WSB are compared. Isoform switched analysis unveiled that *Ncoa4* was not only downregulated but also switched in isoforms was found after axotomy (Figure 7I). *Ncoa4* was recently associated with ferritinophagy and neurodegeneration (Quiles Del Rey and Mancias, 2019).

A comparison of axonal regrowth of primary cortical neurons from P5 newborn B6 or WSB mice confirmed that the differences in growth post-injury seen in mESC derived neurons reflected the regrowth capacity of neurons isolated directly from the postnatal brain (Figure 7J).

Using the RNA-seq data, we analyzed the effect of ID-8 treatment independently of the cell strain, and also compared across the two strains independently of the treatment, throughout all stages analyzed. Analyzing effects of ID-8 in a strain independent fashion, we found only 15 DEG genes, but the cross-strain comparison independent of treatment found 261 DEG (Figure S5A). Similar to the gene expression differences, differential use of transcript variants were found between strains, and our data indicated that in general, the consequences of isoform switches in WSB resulted in shorter transcripts (Figure S5B). It is worth pointing out that *Gapdh,* a housekeeping gene commonly used to normalize expression data, was differentially expressed between WSB and B6 regardless of treatment (Figure S5C). This disparity could be associated with differences in metabolic demands and energetic substrates. The latter correlates with differences we observed in other ontologies like mitochondrial respiratory chain complex II assembly and monocarboxylic acid metabolic process (data not shown). A gene set more enriched in B6 independently of treatment was the regulation of apoptotic process involved in development, whereas that a cerebral cortex development gene set was differentially affected by ID-8, B6 being more severely affected (Figure S5D).

Heterozygous loss of Dyrk1a is lethal on the B6 background but not on 129 or A/J

Finally, we sought to establish the relationship between the *in vitro* susceptibility of B6 to DYRK1A inhibition and the *in vivo* effects of *Dyrk1a* heterozygosity. We generated a null allele of *Dyrk1a* by crossing female mice carrying the germline CMV-Cre to male *Dyrk1a* mice carrying the conditional allele of *Dyrk1a* (floxed *Dyrk1a*) (Figure 8A). We did not recover any live pups heterozygous for *Dyrk1a* deletion (*Dyrk1*a+/-) from this cross (0/93). We were able to obtain several mosaic offspring for the floxed and deleted alleles, but crossing male mosaic mice to WT B6 mice did not produce any live *Dyrk1a*+/- pups (0/46). Given that the prototype mouse model of *Dyrk1a* haploinsufficiency was maintained on a mixed B6/129 background, and our finding that B6 neural progenitors were uniquely sensitive to DYRK1A inhibition, we reasoned that mice carrying the deleted allele may survive on a different background. To test this idea, we crossed male mosaic mice to 129S1 female mice and obtained live *Dyrk1a*+/- mice on a mixed 129/B6 background. We then backcrossed *Dyrk1a*+/- mice to 129S1 for six generations and found that heterozygote and null mutant animals were born at Mendelian ratios. We also mated B6 *Dyrk1* mosaic to AJ females, and live *Dyrk1a* heterozygous pups were born. These results indicate that heterozygous deletion of *Dyrk1a* causes early lethality on the B6 background but does not affect survival on the 129S1 or AJ background.

We further examined the phenotype of *Dyrk1a*$^{+/-}$ mice on the 129B6F1 background. Western blot analyses showed that the level of DYRK1A protein was reduced by half in *Dyrk1a*$^{+/-}$ mice (Figure 8B). Mutant mice appeared smaller and weighed 25% less than WT littermates during postnatal development and as young adults (Figure 8C & D). Likewise, the brains of *Dyrk1a*$^{+/-}$ mice appeared smaller and weighed 30% less than those of control littermates (Figure 8E & F), although the brain to body ratio was not significantly changed. Brain histology indicated that the reduction in brain size was not uniform across the brain, with the mid and hindbrain regions showing larger reductions than the cerebral cortex (Figure 8G). These results corroborate previous findings that heterozygous deletion of *Dyrk1a* in the mouse causes growth retardation and microcephaly, two key clinical features associated with *DYRK1A* mutations in humans. *Dyrk1a*$^{+/-}$ mice on the 129B6F1 background also showed abnormal behaviors. In the open field apparatus, *Dyrk1a*$^{+/-}$ mice were hypoactive compared with WT littermates (Figure 8H); they also spent less time in the center of the arena than WT littermates (Figure 8I), suggesting higher levels of anxiety in the mutant mice. Together, these findings that heterozygous deletion of *Dyrk1a* recapitulates key features of human disease phenotypes, and that the B6 genetic background confers sensitivity to the haploinsufficiency syndrome in the mouse.

Discussion

To facilitate genetic analysis *in vitro* of neural development across a diverse range of mouse genetic backgrounds, we previously developed a new protocol to differentiate pluripotent stem cells into neurons from genetically diverse mESC and hPSC. This is the first protocol that allows for robust neuronal differentiation between genetically diverse strains and across species, both in 2-D or as cerebral organoids.

We demonstrated the applicability of this model in analyzing the effects of chemical knockdown of the activity of a key neurodevelopmental gene throughout neurogenesis and neural maturation and repair, and we were able to demonstrate how the knockdown phenotype varies dramatically depending on the genetic background. As proof of concept, we studied the effects of the inhibition of DYRK1A because it is a kinase that plays multiple roles during the entire ontogeny of neurons, with different effects on each stage of development, and because its haploinsufficiency leads to microcephaly and autism spectrum disorder. Genetic background is known to affect the phenotype of heterozygous loss of function of *DYRK1A* in human (Earl et al., 2017; Murray et al., 2017). Our approach allows the researcher to dissect each step of development in a fast and relatively inexpensive fashion on multiple genetic backgrounds compared to an *in vivo* study. It also permits the study of the early stages of differentiation that are difficult to analyze in the early embryo such as neural specification, or complex conditions in mature neurons such as axonal injury.

By using a selective DYRK1A inhibitor (ID-8) in our model, we were able to recapitulate the effects of *Dyrk1a* haploinsufficiency found in other models and studies. Our studies have revealed that at most stages of this study, from embryonic stem cell renewal to neural specification, neurogenesis, and neural maturation and repair, B6-derived cultures were responsive to DYRK1A inhibition while most other strains proved less sensitive. It is notable that C57BL/6J mice or hybrids thereof have been used successfully in a number of studies to model the effects of DYRK1A haploinsufficiency in human. Thus, on a C57BL/6J, 129S2/SvHsD mixed background, *Dyrk1a*$^{-/-}$ mice show developmental delay and reduced brain size with greatly reduced neuronal content and die at mid-gestation. Heterozygotes on this background have fewer intermediate neural progenitors in the subventricular zone at E11.5-13.5 owing to proliferative defects (Najas et al., 2015). In the adult animal, cortical pyramidal neurons are smaller, and show less branching and fewer spines (Benavides-Piccione et al., 2005), and neural progenitor maintenance in the subventricular zone is impaired (Ferron et al., 2010). These same animals show decreased cognitive abilities (Arque et al., 2008). *Dyrk1a*$^{-/+}$ mice on a pure C57BL/6J background also show reduced brain size and cognitive defects (Raveau et al., 2018). Conditional knockout of *Dyrk1a* in the cortex of C57BL/6J mice was lethal in homozygotes; homozygotes and heterozygotes showed microcephaly related to reduced proliferation of neural progenitors in the immediate postnatal period, and a decreased complexity and reduced branching of cortical neurons (Levy et al., 2021). We could not generate any heterozygous mouse on a pure C57BL/6J, and only when it was crossed with less susceptible strains could we obtain heterozygous mice that showed similar effects to those described by other authors.

Levy et al. used a cortex-specific KO approach which spared the remaining brain and body of the deleterious effects of the KO, making this intervention potentially less lethal. Raveau et al. used a strategy that was not tissue-specific but the target region for the frameshift was upstream of the NLS and in exon 3, whereas in our case it was downstream of the NLS and the kinase domain was targeted. It is possible that in the latter case, the remanent N-terminal peptide can cause a dominant-negative effect generating a more severe phenotype. Interestingly, the finding that *Dyrk1a*$^{-/+}$ had smaller midbrain and hindbrain in our *in vivo* study correlates with aspects of our finding *in vitro*. We found that B6-derived NPCs treated with ID-8 had a decreased expression of *Hoxa4* and *Hoxd3*, homeotic genes associated with hindbrain development. Altogether, our results indicate an impaired development of the hindbrain at an early stage of neural differentiation unveiled by our *in vitro* analysis that otherwise would have been difficult to pinpoint.

Our previous work showed that neural specification of human pluripotent stem cells was blocked in *DYRK1A* knockdown or in ID-8 treated cells (Bellmaine et al., 2017). Here, we showed that the proliferative capacity of neural progenitors derived from *DYRK1A* +/- hPSC was reduced relative to controls. We observed both phenotypes in mESC or mESC-derived neural progenitors from B6 mice. These findings as well as the data discussed above show that our *in vitro* results correctly identify the B6 mouse as a suitable model for the effects of *DYRK1A* haploinsufficiency in the human. By contrast, other strains were unresponsive to the developmental effects of DYRK1A inhibition. We also corroborated the effects of chemical DYRK1A inhibition by conducting knockout experiments demonstrating that the deleterious effect of DYRK1A inhibition is strain dependent. Although *DYRK1A* is subject to strong constraint in the human, and most heterozygotes show impairment of neural development, the severity of clinical phenotypes in individuals hemizygous for loss of the gene varies quite considerably (Earl et al., 2017; Murray et al., 2017). Further *in vitro* analysis of mESC derived from recombinant inbred strains representing sensitive and resistant genetic backgrounds (B6 and 129 respectively) could identify key modifier genes, and potentially target pathways for therapeutic intervention during the early life of affected individuals.

We also examined the effects of DYRK1A inhibition on axonal regrowth across the eight strains in our study. While repair and plasticity processes in the adult CNS often encompass some features of neurodevelopmental pathways, development and repair in the CNS are not identical processes (Li et al., 2010). Our observations showed that the extent of axonal regrowth after injury in neurons derived from mESC does not directly relate to the extent of growth before injury across the mESC lines examined, suggesting that indeed axon growth during development and repair are different even in relatively immature neurons. There were large differences in the ability of axons derived from mESC of different strains to regrow in this assay. Importantly, the robust regrowth of neurons derived from the CAST strain contrasts strikingly with the poor regrowth of neurons derived from B6 mESC. Our observation of poor axonal regrowth in primary cultures of cortical neurons from P5 B6 or WSB mice confirmed the results obtained on neurons derived from mESC. In a number of studies *in vivo*, B6 mice have been shown

to display deficient axonal regeneration relative to 129 or CAST (Basso et al., 2006; Dimou et al., 2006; Kigerl et al., 2006; Ma et al., 2004; Omura et al., 2015; Tedeschi et al., 2017), deficiencies that have been attributed either to variation in the inherent capacity for axonal repair or differences in the extent and nature of inflammatory responses in the various strains.

Comparison of gene expression in B6 and WSB strains that were sensitive or relatively resistant to effects of DYRK1A inhibition across different developmental stages revealed the power of the mESC model to identify critical molecular pathways and networks that are altered by genetic deletion of *Dyrk1A in vivo*. At the stage of neurogenesis, analysis of DEG highlighted the LIF pathway, which is a major regulator of neural progenitor proliferation *in vivo*. RTNA found that networks related to *Foxb1*, a gene critical in the regulation of neural progenitor proliferation, were differentially active in the two strains. Analysis of the expression of splice isoforms showed global changes in the presence of ID-8, in line with the known interactions of DYRK1A with splicing factors. The shift in isoform usage of the BDNF receptor *Ntrk2* to a form encoding a protein lacking the kinase domain in the presence of ID-8 in B6 neural progenitors could explain the downregulation of the BDNF pathway activity observed in a proteomics and phosphoproteomics study of conditional knockout of *Dyrk1a* in the cortical neurons of C57BL/6J mice (Levy et al., 2021). Our studies of axonal repair identified the *Ascl1* regulon as a major differential response to injury in both strains either with or without DYRK1A inhibition. In a model of peripheral neuron (dorsal root ganglion) repair, Lisi et al. (Lisi et al., 2017) noted a differential upregulation of *Ascl1* in CAST (identified by these authors and by our study as a good regenerator compared to B6) relative to B6. These authors also used overexpression and knockdown studies to confirm a role for *Ascl1* in axon regrowth. In summary, our *in vitro* studies comparing gene expression in strains sensitive and resistant to DYRK1A inhibition corroborate *in vivo* data on key molecular pathways involved in neuronal development and repair and their perturbations in *Dyrk1a*-deficient animals.

In our comparison of gene expression in both strains across all stages, the finding that *Gapdh* was the highest DEG was surprising, because it has been widely used as a reference housekeeping gene, with some studies supporting such use (Panina et al., 2018) and others reaching the opposite conclusion (Roy et al., 2020). GAPDH induces apoptosis when translocated into the nuclei of both neural and non-neural cells, and it shows dynamic changes in neurodegenerative diseases, cancer, and hypoxia (Sawa et al., 1997; Tanaka et al., 2002). GAPDH acts a sensor of NO stress (Hara et al., 2006), and participates in dendrite development (Lee et al., 2016; Sawa et al., 1997; Tanaka et al., 2002). The strain differences we observed in *Gapdh* expression could have broader implications for disease modeling in B6 mice.

We acknowledge that we did not investigate the gender effect in our study and all stem cells are male-derived. Although ASD has a higher rate of affected males, and *DYRK1A*mutation is one of the causes of ASD (Halladay et al., 2015); *DYRK1A* haploinsufficiency syndrome does not seem to have a gender bias (Meissner et al., 2020). Evaluations of sex-dependent effects can be performed using female-derived stem cells; nonetheless, this is out of the scope of this paper. Also, we found that despite that our

protocol can efficiently differentiate genetically diverse stem cells, electrical maturation is achieved at different time rates as proven by our MEA recordings. Recently Hergenreder et al. reported that a small molecule cocktail can accelerate neuronal maturation (https://www.biorxiv.org/content/10.1101/2022.06.02.494616v1). Addition of these molecules might synchronize the maturation rate of NPCs from genetically diverse stem cells. Finally, this *in vitro* approach is a facile and cost-efficient tool for first screening of genetic and small molecule interactions.

The approach we describe here could be generalized to address a range of issues in modeling the genetics of disease. We used a specific chemical inhibitor in this study to facilitate screening a panel of mESC at different developmental stages. However, screening approaches using shRNAi or sgRNA CRISPR methodologies are also applicable in this system. We readily applied high content screening and medium throughput microelectrode array methodologies in our work. The small panel of mESC used in this study incorporates wide genetic diversity, but we are also developing mESC or iPSC panels from Diversity Outbred mice and from recombinant inbred strains. These mESC genetic diversity panels have been used for quantitative trait loci analysis, and could be used for rapid mapping of modifiers that influence phenotypes of genetic variants implicated in neurodevelopmental disorders. Identification of modifier genes could yield new leads for drug discovery and early intervention in patients. We focused here on neural development, but this same approach could be applied to any lineage or tissue that can be generated from pluripotent stem cells. Facile comparison between phenotypes of human and mouse pluripotent stem cell models *in vitro* will aid in the identification of those mouse genotypes that confer sensitivity or resilience to disease variants, providing for more precise disease modeling *in vivo* and reducing the experimental use of animals.

Finally, most disease modeling studies using hPSC have been retrospective, replicating the known effects of disease mutations to varying degrees in a culture dish. The use of mESC provides a means for prospective testing of the ability of *in vitro* screens to predict the effects of genetic variants *in vivo*. This will be an important adjunct to hPSC studies aimed at validating novel candidate disease variants emerging from genetic studies in humans. Such a strategy will add considerable power to functional genomics analysis of variants of unknown significance, or variants for which the role in pathogenesis of disease is undefined.

Acknowledgments

This work was supported by the Jackson Laboratory. DEC was the recipient of a JAX Scholar Award. AE was a participant in the JAX Summer Student Program. A National Institutes of Health grant to LGR (U42 OD010921) supported mESC derivation and expansion. We thank Dr. Catherine Kaczorowski for providing access to MEA equipment and for review of the manuscript, and Ms. Anne Czechanski for her advice on mESC culture. Ann Wells, Harshpreet Chandock, and Annat Haber (The Jackson Laboratory) advised on computational analyses. We thank Hong Liu for designing genotyping protocols and genotyping.

Author Contributions

DEC: Conceptualization, Methodology, Validation, Formal Analysis, Investigation, Data Curation, Writing, Visualization, Supervision
ME: Investigation
AM: Investigation, Formal AnalysisACK: Investigation
AE: Investigation
SCM: Formal Analysis, Visualization
SCA: Formal Analysis, Visualization
KMSO: Resources
LGR: Resources, Writing
MFP: Conceptualization, Methodology, Resources, Writing, Supervision. Project Administration, Funding Acquisition

Competing Interests

The authors declare no competing interests.

Figure Legends

Figure 1. *Schematic outline of experiments to study outcome of chemical knockdown of DYRK1A during neural developmental and repair*

Figure 2. *Genotypic and phenotypic analysis of Dyrk1a among the eight CC founder mESC lines.* A) plots depicting the number of SNPs and transcriptional isoforms variants among CC founder mESC compared to the reference genome B6. B) eQTL for both mESC and differentiated NPCs show a peak in the *Dyrk1a* locus representing a local eQTL that can drive differences in expression specially in PWK and CAST. C) pQTL shows no differences in protein expression among all strains analyzed. D-E) Western blot shows protein abundance among mESCs from various strains with no statistically significant differences.

Figure 3. *Effects of DYRK1A inhibition on mESC maintenance and lineage specification vary across genetically diverse mouse strains*. A) Immunofluorescence images showing immunostaining for pluripotency markers in the eight different CC founder mESC cultured in four different culture conditions for four days; B) Heatmaps showing the percentage of cells expressing the markers in the mESCs as measured by HCS; C) Morphometry analysis of the mESCs colonies; D) Comparison of the effects of LIF vs ID-8 treatment on the overall proportion of cells expressing the analyzed markers in the eight different mESCs, determined by HCS. Red indicates decreased percentage of cells expressing the associated marker in ID-8 compared to LIF, green means higher expression. Cell lines and markers are arranged according to the overall degree of change (arrows). *, represents statistically significant differences against the control condition (LIF+2i) within the same cell line. #, represents statistically significant differences among cell lines treated with 2i+LIF and compared to the standard cell line 129. $, represents statistically significant differences among cell lines treated with 2i+ID8 and compared to the standard cell line 129. &, represents statistically significant differences among cell lines treated with LIF and compared to the standard cell line 129. %, represents statistically significant differences among cell lines treated with ID-8 and compared to the standard cell line 129 where a significant difference is indicated when $p < 0.05$. Means +/- SEM are shown. Kruskal-Wallis and Dunn's test were conducted. n = 4 biological replicates.

Figure 4. *DYRK1A inhibition differentially blocks neural progenitor proliferation in a strain-dependent fashion.* A) Representative images of the B6 and WSB mESC lines differentiated into NPCs in the presence of the DYRK1A inhibitor ID-8 and analyzed at day 2, 5 and 8; B) Comparison between the proportion of cells expressing the indicated markers as measured by HCS in control and ID-8 treated cells after eight days of differentiation. Red indicates decreased percentage of cells expressing the associated marker in ID-8-treated cells compared to control whereas green means an increase. Cell lines and markers are arranged according to the overall degree of change (arrows) and n = 4 biological replicates. C and D) Images and plots representing the cell count of proliferating NPCs derived from six independent cell lines different from those used in B.

NPCs were cultured with or without ID-8 for 5 passages. B6 showed a decreased number of cells and proliferative markers (Ki67 and MCM2) compared to its control whereas 129, AJ and, WSB were not affected. n = 4. * Statistically different from its control, $p < 0.05$. Kruskal-Wallis and Dunn's test were conducted E) Long-term proliferation assay in hiPSC-derived NPCs. Cells were kept in proliferative conditions as neurospheres for 15 passages (2 months total). D) Percentage of cells in each cycle phase measured by EdU staining in WT and DYRK1A+/-. Experiment shows DYRK1A +/- NPCs undergo quiescence faster than control. Two-tailed T test, n = 4, * = $p < 0.05$

Figure 5. RNA-seq analysis reveals the genes associated with the impairment in neural induction in B6-derived NPCs. A) Venn diagram of DEG for each set of comparisons. Number in red represents downregulated genes, black indicates upregulated gene; B) RTNA for the top regulons associated with differences in ID- 8 treated WSB- and B6-derived NPCs; C) Barcode plots showing two exemplary GOs differentially affected in WSB and B6 when treated with ID-8. Genes are ranked from left to right by increasing log-fold change represented by the vertical bars. The curve shows the relative local enrichment of the bars in each part of the plot; D) Isoform switch analysis showing the switch in the *Ntrk2* isoform usage when B6 is treated with ID8, upper plot shows the color-coded domains present on each exon (bars). Bar plots indicating total gene expression, isoform expression and relative isoform usage proportional to the total gene expression.

Figure 6 Effect of DYRK1A inhibition on delays in functional maturation of neurons by mESC strain. A) Examples of 30 second recordings of all differentiated neurons (21 and 42 days *in vitro*) in the presence or absence of ID-8; B) Plots for firing rate, number of bursts, interburst interval, synchrony, and spikes per burst. Because the neurons from different strains do not mature and survive equally, data form comparisons among the cell lines were taken at the timepoint where the highest frequency of firing (Hz) was recorded for each cell strain. Means +/- SEM are shown. Kruskal-Wallis and Dunn's test were conducted. * = $p < 0.05$ compared to its own control n = 3 biological replicates. C) Circus plot showing different electrophysiological properties during 42 DIV in the presence of ID-8.

Figure 7. *mESC strain differences in recovery from axonal injury in vitro reflect genetics of recovery from brain injury in vivo*. A) Illustration of the microfluidic chamber used to isolate axons from somas. Image taken from chamber manufacturer webpage; B) representative images of B6, WSB and NZO neurons in microfluidic chambers prior to injury, post-injury in the absence of ID-8, and post-injury in the presence of ID-8; C) heatmap for the area occupied by axons in the chamber two (axonal side) before and after injury; D) Ratio of axonal growth compared to pre-injury in both control and treated neurons. Dunnet's test was used for statistical analysis on three biological replicates; E) MDS plot showing the differences between cell lines over all three conditions; F) Bar plots showing GO analysis of differential response to axonal injury between WSB and B6 in the absence or presence of ID-8; G) RTNA showing the top three regulons associated with the differences between WSB and B6 when axons are injured; H) Enrichment analysis and comparison of isoform switches between the differences in axonal recovery between

B6 and WSB treated or not treated with ID8; I) The isoform switch in the *Ncoa4* gene; J) Axonal recovery experiment conducted on isolated primary cortical neurons from B6 and WSB postnatal day five mice. t-test for statistical analysis on three biological replicates.

Figure 8. Heterozygous deletion of Dyrk1a confirms lethality on the B6 background and causes growth retardation, microcephaly, and abnormal behavior in a mixed background. A) Generation of the null allele of *Dyrk1a* using a conditional *Dyrk1a* allele and constitutively expressed *Cre*. Exons 5 and 6 of Dyrk1a, which encode part of the kinase domain, are flanked by loxP sites. The germline CMV Cre driver removes exons 5 and 6 and the Pgk-Neo selection cassette and causes a frameshift. B-I) Phenotype of *Dyrk1a* heterozygotes in B6/129 background. B) Western blot of cortical tissues from WT and Dyrk1a$^{+/-}$ mice. α-Tub, α-tubulin. C) A Dyrk1a$^{+/-}$ mouse and a WT littermate at 12 weeks of age. D) Body weight of male mutant and control mice at 3 and 12 weeks of age. E) Brains of a control and mutant at 12 weeks of age. F) Brain weights of mutant and control mice at 12 weeks of age. G) sagittal brain sections from a WT and *Dyrk1a*$^{+/-}$ mouse at 3 months of age. Scale bar, 2 mm. H) distance travelled by *Dyrk1a*$^{+/-}$ (n = 7) and WT (n = 7) mice per five minutes in an open field apparatus. I) Percentage of time spent at the center of the arena. * $p < 0.05$, ** $p < 0.01$, *** $p < 0.001$.

STAR Methods

RESOURCE AVAILABILITY

LEAD CONTACT

Further information and requests for resources and reagents should be directed to and will be fulfilled by the lead contact, Martin Pera (martin.pera@jax.org).

MATERIALS AVAILABILITY

This study did not generate new unique reagents.

DATA AND CODE AVAILABILITY

- Bulk RNA-seq data have been deposited at GEO and are publicly available as of the date of publication. Accession numbers are listed in the key resources table.
- This paper does not report original code.
- Any additional information required to reanalyze the data reported in this paper is available from the lead contact upon request

EXPERIMENTAL MODEL AND SUBJECT DETAILS

ANIMALS

Experiments were conducted in accordance with the guidelines of the Institutional Animal Care and Use Committee (IACUC) of the Jackson Laboratory. For axonal injury/recovery experiments in postnatal neurons, postnatal mice (p3-p5) from C57BL/6J and WSB/EiJ strains were sacrificed by decapitation and cells prepared according to the method below (Preparation of p5 NPC for axonal damage experiments).

CELL LINES

mESC from the CC founders (Chesler et al., 2008) were used; however, PWD/PhJ was substituted for PWK/PhJ. All mESCs were kept and used under ten passages to avoid chromosomal rearrangements. All mESCs are male, germ competent, negative for mycoplasma, and retain a normal karyotype. Mouse stem cell media comprised Knockout DMEM, 15% Fetal calf serum, 2 mM Glutamax , non-essential amino-acids, 50 units/ml Penicillin, 50 μg/ml Streptomycin, 55 μM beta-mercaptoethanol, and 1000 IU of Leukemia inhibitory factor. Cells were grown on gamma-irradiated mouse embryonic fibroblast feeder cells at 37°C and 5% CO2. mESCs were passed using Trypsin 0.25%

KOLF2.1J hiPSC is a cell line that was used for neural differentiation studies comparing WT and heterozygous knock-out cells. CRISPR-Cas9 was used to produce frameshift mutants in Exon 2 on one allele of the *DYRK1A* gene, generating Dyrk1a +/- mutants, as previously described ((Andersson-Rolf et al., 2017). Cells were maintained on vitronectin-coated dishes in Stemflex media (Stem Cell Technologies) and passed using ReLSR (Stem Cell Technologies). hPSCs were kept and used under ten passages to avoid chromosomal rearrangements. hPSCs used in this study were karyotyped for chromosomal abnormalities and mycoplasma tested.

METHOD DETAILS

Cortical neuron differentiation of mESCs

mESCs were cultured as described above. Upon reaching 80% confluency (day 0), cells were trypsinized and seeded on a culture dish for an hour to let feeders attach to the dish. Unattached mESCs were recovered and counted. EBs were formed by seeding 300,000 cells on a well of a 6-well plate (ultra-low attachment) in mESC media (described above in "CELL LINES") plus 10 μM SB431542 and 1 μM Dorsomorphin. The next day (day 1), the EBs-containing media was transferred to adherence; previously, a well of a 6-well plate was coated with 100 μg/mL Poly-Lysine (PLL) for 2 hours and then treated with, 1 μg/mL laminin (Lm), 5 μg/mL fibronectin (Fn) for at least two more hours. After 24h (day 2) of seeding the EBs on adherance, media was removed and switched to NMM (Gaspard et al., 2009) (Neurobasal and DMEM/F12 1:1 vol/vol) plus SB431542, Dorsomorphin, 2 μM I-BET151, and 5 μM retinoic acid. 24h later (day 3), media was removed, and fresh NMM plus SB431542 and Dorsomorphin were added. The next day (day 4) SB431542 and Dorsomorphin were withdrawn for B6 and WSB, while the other strains were maintained on SB431542 and Dorsomorphin for two more days (until day 6) after which the inhibitors were withdrawn. Thereafter, all cells were kept on basal media (NMM) with daily media changes until day eight, when cells were passed to the NPC **expansion stage** (day 8 to 11). Dissociation of cells into small clumps was done using Tryple Express and expanded at a 1:2 split ratio on PLL/Fn/Lm-coated dishes in NMM plus 20 ng/mL FGF2, 20 ng/mL EGF, and RevitaCell (Gibco). After 24 hours (day 9), Revitacell is removed but mitogens are daily added for two more days. At day 11, cells were dissociated with Tryple Express to yield a pure population of **NPCs**. NPCs were frozen using Knockout Serum Replacement and 10% DMSO, or passed onto a newly coated plate for **neuronal maturation** using adult NMM media (formulated with Neurobasal A in place of Neurobasal medium), plus Revitacell, 10 ng/mL GDNF, 10 ng/mL BDNF, and 10 μM Forskolin. Next day (day 12) Revitacell was removed. Three days later (day 15), Forskolin was removed and 5 μM 5-fluorodeoxyuridine was added for one week (until day 22). After that, adult-NMM + GDNF and BDNF was changed twice per week.

hPSC-derived NPCs

The protocol is the same as the one used for mESC (Cortes et al. unpublished) but with a few differences. IBet151 and RA are added at day one instead of day two (still 24h treatment). SB431542, and Dorsomorphin are added until day eight. From day eight to eleven, cells were kept in basal NMM media. At day 11, the already differentiated NPCs were passed and expanded using bFGF and EGF for three days. Afterwards, cells were frozen or used for further experiments.

hPSC Neurosphere assay

human NPCs were seeded on a 96-well ultra-low attachment plate at various concentrations (2, 8, 16 and 32 thousand cells) for 15 passages in NMM + FGF2 and EGF. Media changes were performed every other day. Spheroids were imaged with a Leica Dmi1 microscope and their

size calculated using ImageJ software. Spheroids were passed every 4 days using Accutase for 30min at 37°C.

EdU labelling of NPCs

Cells were incubated for 2 hours with 5μM EdU. After 48 hours, cells were harvested and fixed with 4% paraformaldehyde at room temperature for 15 minutes. EdU incorporation was detected according to the Clik-iT EdU Alexa Fluor 594 flow cytometry assay kit protocol. Cells not labelled with EdU were used as negative control.

Electrophysiological Recordings

NPCs were seeded on a previously coated MEA plate and left to mature as described above. However, for the MEA plates, a 10 μl droplet containing 50,000 mouse NPCs or 20,000 human NPCs was seeded at the center of each well of a 48-well plate (CitoView MEA 48, Axion biosystems). After cells have attached (≈7h), more media was added to properly cover the well. Recordings were obtained on day 7, 14, 21, 28, 35, and 42. Spontaneous activity was recorded on an Axion Maestro Pro at 37°C for 10 minutes using the AxiS navigator software. Recordings were analyzed using the built-in spike detector at 6 x STD.

Axonal Damage using mESC-derived neurons

NPCs of each cell line were seeded on one of the two chambers of a microfluidic device (ENUVIO). Devices were pre-coated with PLL/Fn/Lm. Cells were left to mature for four days. Afterwards, in the contralateral chamber, axons were cut off by scratching the chamber and pipetting the media up and down several times. The axonal chamber was rinsed to removed debris and replenished with fresh media and Fn/Lm to enhance axonal attachment. Four days later, the axonal side was treated with Calcein AM, and images of the entire device were taken. The area covered by axons was analyzed using ImageJ.

Preparation of p5 NPC for axonal damage experiments

C57BL/6J (B6) and WSB/EiJ (WSB) postnatal day five animals were euthanized as described above. The hippocampus/dentate gyrus was dissected, mechanically dissociated, and seeded on PLL/Fn/Lm-coated dishes in NMM media plus EGF and FGF (20 μg/ml each) and expanded through one passage. At this point, expanded NPCs were used for axonal damage experiments in the same fashion as mESC-derived NPCs described above.

Immunostaining

Cultures were washed with PBS and fixed with 4% paraformaldehyde 4% for 15 min and finally washed again with PBS three more times. Blocking and permeabilization were carried out using 5% BSA and 0.3% Triton-X for an hour at room temperature. Primary antibodies used were OTX2, Millipore AB9566-1 (1:1000); TUBB3, Biolegend 801202 (1:1000); Ki67, Santa Cruz SC-23900 (1:50); PAX6, Biolegend 862001 (1:1000); Brachyury, R &D systems AF2085 (1:200); Vglut, Abcam ab104898 (1:200); CHAT, Merck Millipore AB144P (1:200); Hb9, Thermo PA5-67195 (1:200); MCM2, Abcam ab95361 (1:500); DYRK1A, cell, signaling, (1:1000); ISL1, DSHB 40.3A4-S and 40.2D6-S both undiluted 1:1; SOX2, Millipore AB5603 (1:500); Eomes, Abcam ab23345 (1:1000); POU5F1, BD 611202 (1:500); GATA4, Santa Cruz SC-25310 (1:2000);

NANOG, PeproTech 500-P236-50UG (1:500); SOX1, R & D AF3369-SP (1:500); AFP, Dako A0008 (1:500); GFAP, Dako Z0334 (1:1000); NeuroD1, Abcam ab60704 (1:2000); TH, Pel-Freez P41301 (1:1000); GAD 65/67, Millipore ABN904 (1:250); vgat, Synaptic systems 131011 (1:200); Reelin, Abcam ab78540 (1:200). Primary antibodies were incubated overnight, washed three times with PBS and secondary ALEXA antibodies (1:1000) against primary antibodies were incubated for two hours. DAPI was used for nuclear counterstaining. Cerebral organoids were cleared and stained using fructose-glycerol clearing method (Dekkers et al., 2019) and antibodies were used at twice the concentrations described above.

High content microscopy

Perkin Elmer cell carrier ultra 96-well plates were used for high content microscopy. Imaging was carried out on the Operetta CSL (Perkin Elmer) microscope, and image analysis was done using Harmony software.

RT-PCR

Samples were collected and RNA was prepared using Qiagen RNAeasy plus mini kit (Qiagen). Reverse transcription was carried out using High-Capacity RNA-to-cDNA™ Kit (ThermoFisher). Real-time PCR was conducted using Quantstudio 7 Flex on a 2-step cycle run using Taqman Probes (Oct4, # 4331182; Nanog, #4331182; Otx2, #4331182; Pax6, #4331182; Tubb3, #4351372; Scl17a7, # 4331182; Gapdh, # 4453320).

Bulk RNA-seq

Samples were collected and RNA was prepared using Qiagen RNA column system. mRNA libraries were made at 150 x2 with at least 30 000 reads per sample.

Transcriptomic analysis

Low-quality bases (Q < 30) from the 3' end of reads were removed and reads with more than 30% low-quality bases (Q < 30) overall were filtered out. Trimmed reads were aligned to the reference genome using bowtie2 (Wei et al., 2018), generating a bam file which was used by rsem for quantification providing expression counts for genes and isoforms separately. Quality metrics were obtained at the fastq and bam level. This includes metrics such as total number of reads, total number of high-quality reads and alignment rate. The RNA-seq data was filtered and normalized. MDS plots were made using EdgeR (Robinson et al., 2010). Venn diagrams were made using systemPipeR (TW and Girke, 2016) and the Limma (Ritchie et al., 2015) package was used for barcode plots and testing for multiple gene sets. Gene ontology analysis and plotting was completed using TopGO (Alexa A, 2020) and GO.db (M, 2019). Transcriptional network analysis was done using RTN (Fletcher et al., 2013). Circos plots were made using circlize (Gu et al., 2014). Isoform switching was analyzed using IsoformSwitchAnalyzeR package (Vitting-Seerup et al., 2014) and other tools to import data, conduct normalization, isoform switch testing, prediction of open reading frames, premature termination decay, coding, domaings signal peptides, protein disorder and consequences (Almagro Armenteros et al., 2019; Finn et al., 2010; Huber et al., 2015; Meszaros et al., 2018; Vitting-Seerup et al., 2014; Vitting-Seerup and Sandelin, 2019; Wang et al., 2013)

Statistical analysis

Statistical details can be found within the figure legends. Computation and plots were done using Rstudio and GraphPad Prism.

SNP and transcript variant analysis
Dyrk1a sequences were pulled from the mouse genome project (https://www.mousegenomes.org/) and compared for number of SNPs and transcript variants per strains. Sequence variants were aligned using Clustal O multiple sequence alignment. Sequences downloaded from https://www.informatics.jax.org/mgv/

QTL analysis

Diversity outbred (DO) mouse embryonic stem cell (mESC) expression quantitative trait loci (eQTL) and protein QTL analysis are previously published (Skelly et al,. 2020 and Aydin et al., 2023) and available at (https://churchilllab.jax.org/qtlviewer/DO_mESC and https://doi.org/10.6084/m9.figshare.22012850). Data for Dyrk1a was accessed through publicly available data sources. QTL mapping was performed using a linear-mixed model implemented in the 'scan1' function in R/qtl2 package with rank normal scores, sex of the cell lines as an additive covariate and the leave one chromosome out option for kinship correction (citations for R/qtl2 and DOQTL).

Western blot
Cells were lysed with NP40 cell lysis buffer. Including Protease Inhibitor Cocktail-P2714, Sigma. Cells were centrifuged for 15 min at 12,000g at 4°C. Supernatant was saved and kept frozen until further use. DC protein assay (Bio-Rad) was used to quantify protein. Cell lysate was placed in SDS sample buffer and used as it is. Samples were run in a pre-casted gel at 100V. Protein were transferred into nitrocellulose using the trans-Blot turbo (BIO-RAD). Primary antibodiesare described above. Secondary antibodies goat anti-Rb HRP (Abcam ab6721, 1:10,000) and horse anti-ms (Vector Labs PI-2000-1). Detection was performed using SuperSignal Atto (Thermo) using a G box documentation system (Syngene)

Generation of *Dyrk1a* null allele
Mice carrying *Dyrk1a* null allele were generated by mating male mice homozygous of conditional *Dyrk1a* floxed allele (JAX Strain #027801) with female mice hemizygous of the germline CMV-Cre (JAX Strain #006054). Both strains were on a B6 background. Genotyping was performed by PCR on tail DNA. The PCR primers for Dyrk1a alleles are: forward 5'-CCT GGA GAA GAG GGC AAG-3' (common), reverse 5'-GGC ATA ACTTGC ATA CAG TGG-3' (wild type and floxed allele), and reverse 5'-ACT GTG TGA GGA GTC TTG ACA-3' (null allele), which give products of 132, 232 and 295 bp for wild type, floxed, and null allele, respectively. The PCR primers for CMV-Cre are: forward 5'-GCA TTA CCG GTC GAT GCA ACG AGT GAT GAG-3', reverse 5'-GAG TGA ACG AAC CTG GTC GAA ATC AGT GCG-3', which gives a product of 410 bp for the transgene.

The cross between floxed *Dyrk1a* and CMV-Cre on B6 background did not produce any pups heterozygous of Dyrk1a null allele (0/93 pups), but a few live pups were mosaic for floxed and null allele. Crossing male mosaic mice to wild type B6 females did not produce any pups (0/46 pups). In contrast, crossing the same male mosaic mice to wild type 129S1 females produced

live pups heterozygous of *Dyrk1a* null allele (*Dyrk1a+/-,* 15/81 pups). Further backcrossing to 129S1 produced *Dyrk1a*+/- mice at Mendelian ratios.

Phenotyping of *Dyrk1a* +/- mice

Mice on 129B6 F1 background were used for phenotyping. Western blots were performed with cortical tissues obtained from *Dyrk1a*+/- and wild type mice at 13 weeks of age, using standard procedures and antibodies against DYRK1A (Cell Signaling #8756, 1:1000) and α-tubulin (ThermoFisher #A11126, 1:5000, loading control). Protein levels were quantified using ImageJ. For each sample, DYRK1A protein level was normalized to that of α-tubulin.

Activity of mice was analyzed at 10 to 12 weeks of age with an open field apparatus where a single mouse was allowed to explore freely for 30 min and recorded by video. Activity was analyzed using idTracker (Perez-Escudero et al., Nature Methods, 2014). Distance travelled per 5 min and time spent in the center square were quantified.

For brain weight and morphology, mice were euthanized at 12 weeks of age and perfused with 4% paraformaldehyde. Whole brains were dissected and weighted. Brain sections were cut at 70 μm thickness and stained with H&E method.

Dyrk1a knockout mESCs

C57Bl6/J embryonic stem cells (line #49) were grown on irradiated MEFs in 2i/FCS/LIF media (Czechanski et al. 2014). Exon 3 of *Dyrk1a* (Dyrk1a-202, ENMUST00000119878) was deleted in ESCs using CRISPR/Cas9. Briefly, oligos encoding guide RNAs targeting intron 2 and intron 3 of murine *Dyrk1a* were cloned into plasmid pX459 v2.0 (Addgene plasmid # 62988) and sequence verified. Plasmids encoding *Dyrk1a* sgRNAs were transfected into mouse ESCs using Lipofectamine 3000 (Life/Thermo) at a ratio of 1 ug total plasmid per 200,000 cells. After 24 hours, cells were transferred to irradiated DR4 puromycin-resistant MEFs and transfected cells were selected for 40 hours with 1 ug/ml puromycin. Cells were then removed from puromycin selection and cultured for 1 week, then individual colonies were picked into 96 well plates. Clones were genotyped by PCR with primers Dyrk1a_For (5'-CATTCCATGCTGCTGGCCTTC-3') and Dyrk1a_Rev: 5'-GCCAGCAGCATGGAATGAGAAC-3') and analyzed by gel electrophoresis. Clones completely missing a wildtype band (1712 bp) were further expanded and re-genotyped for confirmation of loss of exon 3.

References

Alexa A, R.J. (2020). topGO: Enrichment Analysis for Gene Ontology. R package version 2.42.0.
Alexander, T., Nolte, C., and Krumlauf, R. (2009). Hox genes and segmentation of the hindbrain and axial skeleton. Annu Rev Cell Dev Biol *25*, 431-456.
Almagro Armenteros, J.J., Tsirigos, K.D., Sonderby, C.K., Petersen, T.N., Winther, O., Brunak, S., von Heijne, G., and Nielsen, H. (2019). SignalP 5.0 improves signal peptide predictions using deep neural networks. Nat Biotechnol *37*, 420-423.
Alvarez, M., Estivill, X., and de la Luna, S. (2003). DYRK1A accumulates in splicing speckles through a novel targeting signal and induces speckle disassembly. J Cell Sci *116*, 3099-3107.
Andersson-Rolf, A., Mustata, R.C., Merenda, A., Kim, J., Perera, S., Grego, T., Andrews, K., Tremble, K., Silva, J.C., Fink, J.*, et al.* (2017). One-step generation of conditional and reversible gene knockouts. Nat Methods *14*, 287-289.
Arbones, M.L., Thomazeau, A., Nakano-Kobayashi, A., Hagiwara, M., and Delabar, J.M. (2019). DYRK1A and cognition: A lifelong relationship. Pharmacol Ther *194*, 199-221.
Arque, G., Fotaki, V., Fernandez, D., Martinez de Lagran, M., Arbones, M.L., and Dierssen, M. (2008). Impaired spatial learning strategies and novel object recognition in mice haploinsufficient for the dual specificity tyrosine-regulated kinase-1A (Dyrk1A). PLoS One *3*, e2575.
Aydin, S., Pham, D.T., Zhang, T., Keele, G.R., Skelly, D.A., Paulo, J.A., Pankratz, M., Choi, T., Gygi, S.P., Reinholdt, L.G.*, et al.* (2023). Genetic dissection of the pluripotent proteome through multi-omics data integration. Cell Genom *3*, 100283.
Basso, D.M., Fisher, L.C., Anderson, A.J., Jakeman, L.B., McTigue, D.M., and Popovich, P.G. (2006). Basso Mouse Scale for locomotion detects differences in recovery after spinal cord injury in five common mouse strains. J Neurotrauma *23*, 635-659.
Bellmaine, S.F., Ovchinnikov, D.A., Manallack, D.T., Cuddy, C.E., Elefanty, A.G., Stanley, E.G., Wolvetang, E.J., Williams, S.J., and Pera, M. (2017). Inhibition of DYRK1A disrupts neural lineage specificationin human pluripotent stem cells. Elife *6*.
Benavides-Piccione, R., Dierssen, M., Ballesteros-Yanez, I., Martinez de Lagran, M., Arbones, M.L., Fotaki, V., DeFelipe, J., and Elston, G.N. (2005). Alterations in the phenotype of neocortical pyramidal cells in the Dyrk1A+/- mouse. Neurobiol Dis *20*, 115-122.
Branca, C., Shaw, D.M., Belfiore, R., Gokhale, V., Shaw, A.Y., Foley, C., Smith, B., Hulme, C., Dunckley, T., Meechoovet, B.*, et al.* (2017). Dyrk1 inhibition improves Alzheimer's disease-like pathology. Aging Cell *16*, 1146-1154.
Chandler, C.H., Chari, S., and Dworkin, I. (2013). Does your gene need a background check? How genetic background impacts the analysis of mutations, genes, and evolution. Trends Genet *29*, 358-366.
Chesler, E.J., Miller, D.R., Branstetter, L.R., Galloway, L.D., Jackson, B.L., Philip, V.M., Voy, B.H., Culiat, C.T., Threadgill, D.W., Williams, R.W.*, et al.* (2008). The Collaborative Cross at Oak Ridge National Laboratory: developing a powerful resource for systems genetics. Mamm Genome *19*, 382-389.
Cortes, D., and Pera, M.F. (2021). The genetic basis of inter-individual variation in recovery from traumatic brain injury. NPJ Regen Med *6*, 5.
Czechanski, A., Byers, C., Greenstein, I., Schrode, N., Donahue, L.R., Hadjantonakis, A.K., and Reinholdt, L.G. (2014). Derivation and characterization of mouse embryonic stem cells from permissive and nonpermissive strains. Nat Protoc *9*, 559-574.
Dang, T., Duan, W.Y., Yu, B., Tong, D.L., Cheng, C., Zhang, Y.F., Wu, W., Ye, K., Zhang, W.X., Wu, M.*, et al.* (2018). Autism-associated Dyrk1a truncation mutants impair neuronal dendritic and spine growth and interfere with postnatal cortical development. Mol Psychiatry *23*, 747-758.

Desai, S., Ding, M., Wang, B., Lu, Z., Zhao, Q., Shaw, K., Yung, W.K., Weinstein, J.N., Tan, M., and Yao, J. (2014). Tissue-specific isoform switch and DNA hypomethylation of the pyruvate kinase PKM gene in human cancers. Oncotarget *5*, 8202-8210.
Dimou, L., Schnell, L., Montani, L., Duncan, C., Simonen, M., Schneider, R., Liebscher, T., Gullo, M., and Schwab, M.E. (2006). Nogo-A-deficient mice reveal strain-dependent differences in axonal regeneration. J Neurosci *26*, 5591-5603.
Ding, S., Shi, J., Qian, W., Iqbal, K., Grundke-Iqbal, I., Gong, C.X., and Liu, F. (2012). Regulation of alternative splicing of tau exon 10 by 9G8 and Dyrk1A. Neurobiol Aging *33*, 1389-1399.
Earl, R.K., Turner, T.N., Mefford, H.C., Hudac, C.M., Gerdts, J., Eichler, E.E., and Bernier, R.A. (2017). Clinical phenotype of ASD-associated DYRK1A haploinsufficiency. Mol Autism *8*, 54.
Erickson, R.P. (1996). Mouse models of human genetic disease: which mouse is more like a man? Bioessays *18*, 993-998.
Feki, A., and Hibaoui, Y. (2018). DYRK1A Protein, A Promising Therapeutic Target to Improve Cognitive Deficits in Down Syndrome. Brain Sci *8*.
Fernandez-Martinez, P., Zahonero, C., and Sanchez-Gomez, P. (2015). DYRK1A: the double-edged kinase as a protagonist in cell growth and tumorigenesis. Mol Cell Oncol *2*, e970048.
Fernando, M.B., Ahfeldt, T., and Brennand, K.J. (2020). Modeling the complex genetic architectures of brain disease. Nat Genet *52*, 363-369.
Ferron, S.R., Pozo, N., Laguna, A., Aranda, S., Porlan, E., Moreno, M., Fillat, C., de la Luna, S., Sanchez, P., Arbones, M.L.*, et al.* (2010). Regulated segregation of kinase Dyrk1A during asymmetric neural stem cell division is critical for EGFR-mediated biased signaling. Cell Stem Cell *7*, 367-379.
Finn, R.D., Mistry, J., Tate, J., Coggill, P., Heger, A., Pollington, J.E., Gavin, O.L., Gunasekaran, P., Ceric, G., Forslund, K.*, et al.* (2010). The Pfam protein families database. Nucleic Acids Res *38*, D211-222.
Fletcher, M.N., Castro, M.A., Wang, X., de Santiago, I., O'Reilly, M., Chin, S.F., Rueda, O.M., Caldas, C., Ponder, B.A., Markowetz, F.*, et al.* (2013). Master regulators of FGFR2 signalling and breast cancer risk. Nat Commun *4*, 2464.
Garbutt, T.A., Konneker, T.I., Konganti, K., Hillhouse, A.E., Swift-Haire, F., Jones, A., Phelps, D., Aylor, D.L., and Threadgill, D.W. (2018). Permissiveness to form pluripotent stem cells may be an evolutionarily derived characteristic in Mus musculus. Sci Rep *8*, 14706.
Gu, Z., Gu, L., Eils, R., Schlesner, M., and Brors, B. (2014). circlize Implements and enhances circular visualization in R. Bioinformatics *30*, 2811-2812.
Halladay, A.K., Bishop, S., Constantino, J.N., Daniels, A.M., Koenig, K., Palmer, K., Messinger, D., Pelphrey, K., Sanders, S.J., Singer, A.T.*, et al.* (2015). Sex and gender differences in autism spectrum disorder: summarizing evidence gaps and identifying emerging areas of priority. Mol Autism *6*, 36.
Hara, M.R., Cascio, M.B., and Sawa, A. (2006). GAPDH as a sensor of NO stress. Biochim Biophys Acta *1762*, 502-509.
Hasegawa, K., Yasuda, S.Y., Teo, J.L., Nguyen, C., McMillan, M., Hsieh, C.L., Suemori, H., Nakatsuji, N., Yamamoto, M., Miyabayashi, T.*, et al.* (2012). Wnt signaling orchestration with a small molecule DYRK inhibitor provides long-term xeno-free human pluripotent cell expansion. Stem Cells Transl Med *1*, 18-28.
Huber, W., Carey, V.J., Gentleman, R., Anders, S., Carlson, M., Carvalho, B.S., Bravo, H.C., Davis, S., Gatto, L., Girke, T.*, et al.* (2015). Orchestrating high-throughput genomic analysis with Bioconductor. Nat Methods *12*, 115-121.
Keller, M.P., Gatti, D.M., Schueler, K.L., Rabaglia, M.E., Stapleton, D.S., Simecek, P., Vincent, M., Allen, S., Broman, A.T., Bacher, R.*, et al.* (2018). Genetic Drivers of Pancreatic Islet Function. Genetics *209*, 335-356.

Kigerl, K.A., McGaughy, V.M., and Popovich, P.G. (2006). Comparative analysis of lesion development and intraspinal inflammation in four strains of mice following spinal contusion injury. J Comp Neurol *494*, 578-594.
Lee, F.H., Su, P., Xie, Y.F., Wang, K.E., Wan, Q., and Liu, F. (2016). Disrupting GluA2-GAPDH Interaction Affects Axon and Dendrite Development. Sci Rep *6*, 30458.
Levy, J.A., LaFlamme, C.W., Tsaprailis, G., Crynen, G., and Page, D.T. (2021). Dyrk1a Mutations Cause Undergrowth of Cortical Pyramidal Neurons via Dysregulated Growth Factor Signaling. Biol Psychiatry *90*, 295-306.
Li, H., and Auwerx, J. (2020). Mouse Systems Genetics as a Prelude to Precision Medicine. Trends Genet *36*, 259-272.
Li, S., Overman, J.J., Katsman, D., Kozlov, S.V., Donnelly, C.J., Twiss, J.L., Giger, R.J., Coppola, G., Geschwind, D.H., and Carmichael, S.T. (2010). An age-related sprouting transcriptome provides molecular control of axonal sprouting after stroke. Nat Neurosci *13*, 1496-1504.
Lisi, V., Singh, B., Giroux, M., Guzman, E., Painter, M.W., Cheng, Y.C., Huebner, E., Coppola, G., Costigan, M., Woolf, C.J.*, et al.* (2017). Enhanced Neuronal Regeneration in the CAST/Ei Mouse Strain Is Linked to Expression of Differentiation Markers after Injury. Cell Rep *20*, 1136-1147.
M, C. (2019). GO.db: A set of annotation maps describing the entire Gene Ontology.
Ma, M., Wei, P., Wei, T., Ransohoff, R.M., and Jakeman, L.B. (2004). Enhanced axonal growth into a spinal cord contusion injury site in a strain of mouse (129X1/SvJ) with a diminished inflammatory response. J Comp Neurol *474*, 469-486.
Majer, A., Medina, S.J., Sorensen, D., Martin, M.J., Frost, K.L., Phillipson, C., Manguiat, K., and Booth, S.A. (2019). The cell type resolved mouse transcriptome in neuron-enriched brain tissues from the hippocampus and cerebellum during prion disease. Sci Rep *9*, 1099.
Meissner, L.E., Macnamara, E.F., D'Souza, P., Yang, J., Vezina, G., Undiagnosed Diseases, N., Ferreira, C.R., Zein, W.M., Tifft, C.J., and Adams, D.R. (2020). DYRK1A pathogenic variants in two patients with syndromic intellectual disability and a review of the literature. Mol Genet Genomic Med *8*, e1544.
Meszaros, B., Erdos, G., and Dosztanyi, Z. (2018). IUPred2A: context-dependent prediction of protein disorder as a function of redox state and protein binding. Nucleic Acids Res *46*, W329-W337.
Miyabayashi, T., Yamamoto, M., Sato, A., Sakano, S., and Takahashi, Y. (2008). Indole derivatives sustain embryonic stem cell self-renewal in long-term culture. Biosci Biotechnol Biochem *72*, 1242-1248.
Molenhuis, R.T., Bruining, H., Brandt, M.J.V., van Soldt, P.E., Abu-Toamih Atamni, H.J., Burbach, J.P.H., Iraqi, F.A., Mott, R.F., and Kas, M.J.H. (2018). Modeling the quantitative nature of neurodevelopmental disorders using Collaborative Cross mice. Mol Autism *9*, 63.
Monteiro, M.B., Ramm, S., Chandrasekaran, V., Boswell, S.A., Weber, E.J., Lidberg, K.A., Kelly, E.J., and Vaidya, V.S. (2018). A High-Throughput Screen Identifies DYRK1A Inhibitor ID-8 that Stimulates Human Kidney Tubular Epithelial Cell Proliferation. J Am Soc Nephrol *29*, 2820-2833.
Moore, S.J., Murphy, G.G., and Cazares, V.A. (2020). Turning strains into strengths for understanding psychiatric disorders. Mol Psychiatry *25*, 3164-3177.
Murray, C.R., Abel, S.N., McClure, M.B., Foster, J., 2nd, Walke, M.I., Jayakar, P., Bademci, G., and Tekin, M. (2017). Novel Causative Variants in DYRK1A, KARS, and KAT6A Associated with Intellectual Disability and Additional Phenotypic Features. J Pediatr Genet *6*, 77-83.
Najas, S., Arranz, J., Lochhead, P.A., Ashford, A.L., Oxley, D., Delabar, J.M., Cook, S.J., Barallobre, M.J., and Arbones, M.L. (2015). DYRK1A-mediated Cyclin D1 Degradation in Neural Stem Cells Contributes to the Neurogenic Cortical Defects in Down Syndrome. EBioMedicine *2*, 120-134.

Neuner, S.M., Heuer, S.E., Huentelman, M.J., O'Connell, K.M.S., and Kaczorowski, C.C. (2019). Harnessing Genetic Complexity to Enhance Translatability of Alzheimer's Disease Mouse Models: A Path toward Precision Medicine. Neuron *101*, 399-411 e395.
Nichols, J., Silva, J., Roode, M., and Smith, A. (2009). Suppression of Erk signalling promotes ground state pluripotency in the mouse embryo. Development *136*, 3215-3222.
Ning, S., Pagano, J.S., and Barber, G.N. (2011). IRF7: activation, regulation, modification and function. Genes Immun *12*, 399-414.
Omura, T., Omura, K., Tedeschi, A., Riva, P., Painter, M.W., Rojas, L., Martin, J., Lisi, V., Huebner, E.A., Latremoliere, A.*, et al.* (2015). Robust Axonal Regeneration Occurs in the Injured CAST/Ei Mouse CNS. Neuron *86*, 1215-1227.
Onos, K.D., Uyar, A., Keezer, K.J., Jackson, H.M., Preuss, C., Acklin, C.J., O'Rourke, R., Buchanan, R., Cossette, T.L., Sukoff Rizzo, S.J.*, et al.* (2019). Enhancing face validity of mouse models of Alzheimer's disease with natural genetic variation. PLoS Genet *15*, e1008155.
Ortmann, D., Brown, S., Czechanski, A., Aydin, S., Muraro, D., Huang, Y., Tomaz, R.A., Osnato, A., Canu, G., Wesley, B.T.*, et al.* (2020). Naive Pluripotent Stem Cells Exhibit Phenotypic Variability that Is Driven by Genetic Variation. Cell Stem Cell *27*, 470-481 e476.
Ozdinler, P.H., and Erzurumlu, R.S. (2002). Slit2, a branching-arborization factor for sensory axons in the Mammalian CNS. J Neurosci *22*, 4540-4549.
Panina, Y., Germond, A., Masui, S., and Watanabe, T.M. (2018). Validation of Common Housekeeping Genes as Reference for qPCR Gene Expression Analysis During iPS Reprogramming Process. Sci Rep *8*, 8716.
Pantazis, C.B., Yang, A., Lara, E., McDonough, J.A., Blauwendraat, C., Peng, L., Oguro, H., Kanaujiya, J., Zou, J., Sebesta, D.*, et al.* (2022). A reference human induced pluripotent stem cell line for large-scale collaborative studies. Cell Stem Cell *29*, 1685-1702 e1622.
Quiles Del Rey, M., and Mancias, J.D. (2019). NCOA4-Mediated Ferritinophagy: A Potential Link to Neurodegeneration. Front Neurosci *13*, 238.
Raveau, M., Shimohata, A., Amano, K., Miyamoto, H., and Yamakawa, K. (2018). DYRK1A-haploinsufficiency in mice causes autistic-like features and febrile seizures. Neurobiol Dis *110*, 180-191.
Riordan, J.D., and Nadeau, J.H. (2017). From Peas to Disease: Modifier Genes, Network Resilience, and the Genetics of Health. Am J Hum Genet *101*, 177-191.
Ritchie, M.E., Phipson, B., Wu, D., Hu, Y., Law, C.W., Shi, W., and Smyth, G.K. (2015). limma powers differential expression analyses for RNA-sequencing and microarray studies. Nucleic Acids Res *43*, e47.
Robinson, M.D., McCarthy, D.J., and Smyth, G.K. (2010). edgeR: a Bioconductor package for differential expression analysis of digital gene expression data. Bioinformatics *26*, 139-140.
Roy, J.G., McElhaney, J.E., and Verschoor, C.P. (2020). Reliable reference genes for the quantification of mRNA in human T-cells and PBMCs stimulated with live influenza virus. BMC Immunol *21*, 4.
Sawa, A., Khan, A.A., Hester, L.D., and Snyder, S.H. (1997). Glyceraldehyde-3-phosphate dehydrogenase: nuclear translocation participates in neuronal and nonneuronal cell death. Proc Natl Acad Sci U S A *94*, 11669-11674.
Shi, J., Zhang, T., Zhou, C., Chohan, M.O., Gu, X., Wegiel, J., Zhou, J., Hwang, Y.W., Iqbal, K., Grundke-Iqbal, I.*, et al.* (2008). Increased dosage of Dyrk1A alters alternative splicing factor (ASF)-regulated alternative splicing of tau in Down syndrome. J Biol Chem *283*, 28660-28669.
Shimazaki, T., Shingo, T., and Weiss, S. (2001). The ciliary neurotrophic factor/leukemia inhibitory factor/gp130 receptor complex operates in the maintenance of mammalian forebrain neural stem cells. J Neurosci *21*, 7642-7653.
Sittig, L.J., Carbonetto, P., Engel, K.A., Krauss, K.S., Barrios-Camacho, C.M., and Palmer, A.A. (2016). Genetic Background Limits Generalizability of Genotype-Phenotype Relationships. Neuron *91*, 1253-1259.

Skelly, D.A., Czechanski, A., Byers, C., Aydin, S., Spruce, C., Olivier, C., Choi, K., Gatti, D.M., Raghupathy, N., Keele, G.R.*, et al.* (2020). Mapping the Effects of Genetic Variation on Chromatin State and Gene Expression Reveals Loci That Control Ground State Pluripotency. Cell Stem Cell *27*, 459-469 e458.
Swanzey, E., McNamara, T.F., Apostolou, E., Tahiliani, M., and Stadtfeld, M. (2020). A Susceptibility Locus on Chromosome 13 Profoundly Impacts the Stability of Genomic Imprinting in Mouse Pluripotent Stem Cells. Cell Rep *30*, 3597-3604 e3593.
Swanzey, E., O'Connor, C., and Reinholdt, L.G. (2021). Mouse Genetic Reference Populations: Cellular Platforms for Integrative Systems Genetics. Trends Genet *37*, 251-265.
Tanaka, R., Mochizuki, H., Suzuki, A., Katsube, N., Ishitani, R., Mizuno, Y., and Urabe, T. (2002). Induction of glyceraldehyde-3-phosphate dehydrogenase (GAPDH) expression in rat brain after focal ischemia/reperfusion. J Cereb Blood Flow Metab *22*, 280-288.
Tedeschi, A., Omura, T., and Costigan, M. (2017). CNS repair and axon regeneration: Using genetic variation to determine mechanisms. Exp Neurol *287*, 409-422.
Tejedor, F., Zhu, X.R., Kaltenbach, E., Ackermann, A., Baumann, A., Canal, I., Heisenberg, M., Fischbach, K.F., and Pongs, O. (1995). minibrain: a new protein kinase family involved in postembryonic neurogenesis in Drosophila. Neuron *14*, 287-301.
Togashi, H., Sakisaka, T., and Takai, Y. (2009). Cell adhesion molecules in the central nervous system. Cell Adh Migr *3*, 29-35.
Toiber, D., Azkona, G., Ben-Ari, S., Toran, N., Soreq, H., and Dierssen, M. (2010). Engineering DYRK1A overdosage yields Down syndrome-characteristic cortical splicing aberrations. Neurobiol Dis *40*, 348-359.
TW, H.B., and Girke, T. (2016). systemPipeR: NGS workflow and report generation environment. BMC Bioinformatics *17*, 388.
van de Leemput, J., Boles, N.C., Kiehl, T.R., Corneo, B., Lederman, P., Menon, V., Lee, C., Martinez, R.A., Levi, B.P., Thompson, C.L.*, et al.* (2014). CORTECON: a temporal transcriptome analysis of in vitro human cerebral cortex development from human embryonic stem cells. Neuron *83*, 51-68.
Vitting-Seerup, K., Porse, B.T., Sandelin, A., and Waage, J. (2014). spliceR: an R package for classification of alternative splicing and prediction of coding potential from RNA-seq data. BMC Bioinformatics *15*, 81.
Vitting-Seerup, K., and Sandelin, A. (2019). IsoformSwitchAnalyzeR: analysis of changes in genome-wide patterns of alternative splicing and its functional consequences. Bioinformatics *35*, 4469-4471.
Wang, L., Park, H.J., Dasari, S., Wang, S., Kocher, J.P., and Li, W. (2013). CPAT: Coding-Potential Assessment Tool using an alignment-free logistic regression model. Nucleic Acids Res *41*, e74.
Wei, Z., Zhang, W., Fang, H., Li, Y., and Wang, X. (2018). esATAC: an easy-to-use systematic pipeline for ATAC-seq data analysis. Bioinformatics *34*, 2664-2665.
Ying, Q.L., Wray, J., Nichols, J., Batlle-Morera, L., Doble, B., Woodgett, J., Cohen, P., and Smith, A. (2008). The ground state of embryonic stem cell self-renewal. Nature *453*, 519-523.
Zhang, Y., Hoxha, E., Zhao, T., Zhou, X., and Alvarez-Bolado, G. (2017). Foxb1 Regulates Negatively the Proliferation of Oligodendrocyte Progenitors. Front Neuroanat *11*, 53.

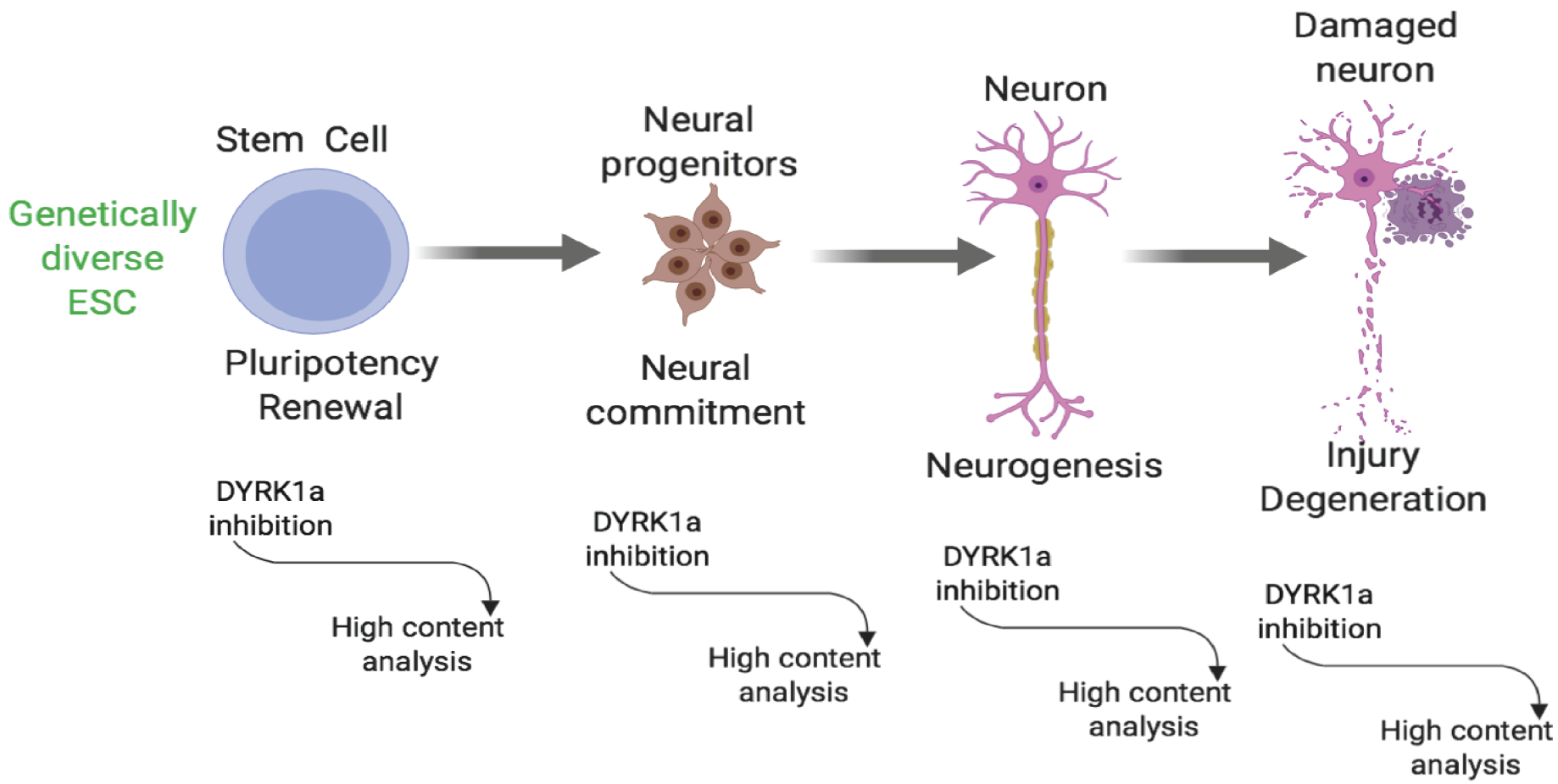
Genetically diverse ESC
Stem Cell
Pluripotency Renewal
Neural progenitors
Neural commitment
Neuron
Neurogenesis
Damaged neuron
Injury Degeneration
DYRK1a inhibition
High content analysis
DYRK1a inhibition
High content analysis
DYRK1a inhibition
High content analysis
DYRK1a inhibition
High content analysis

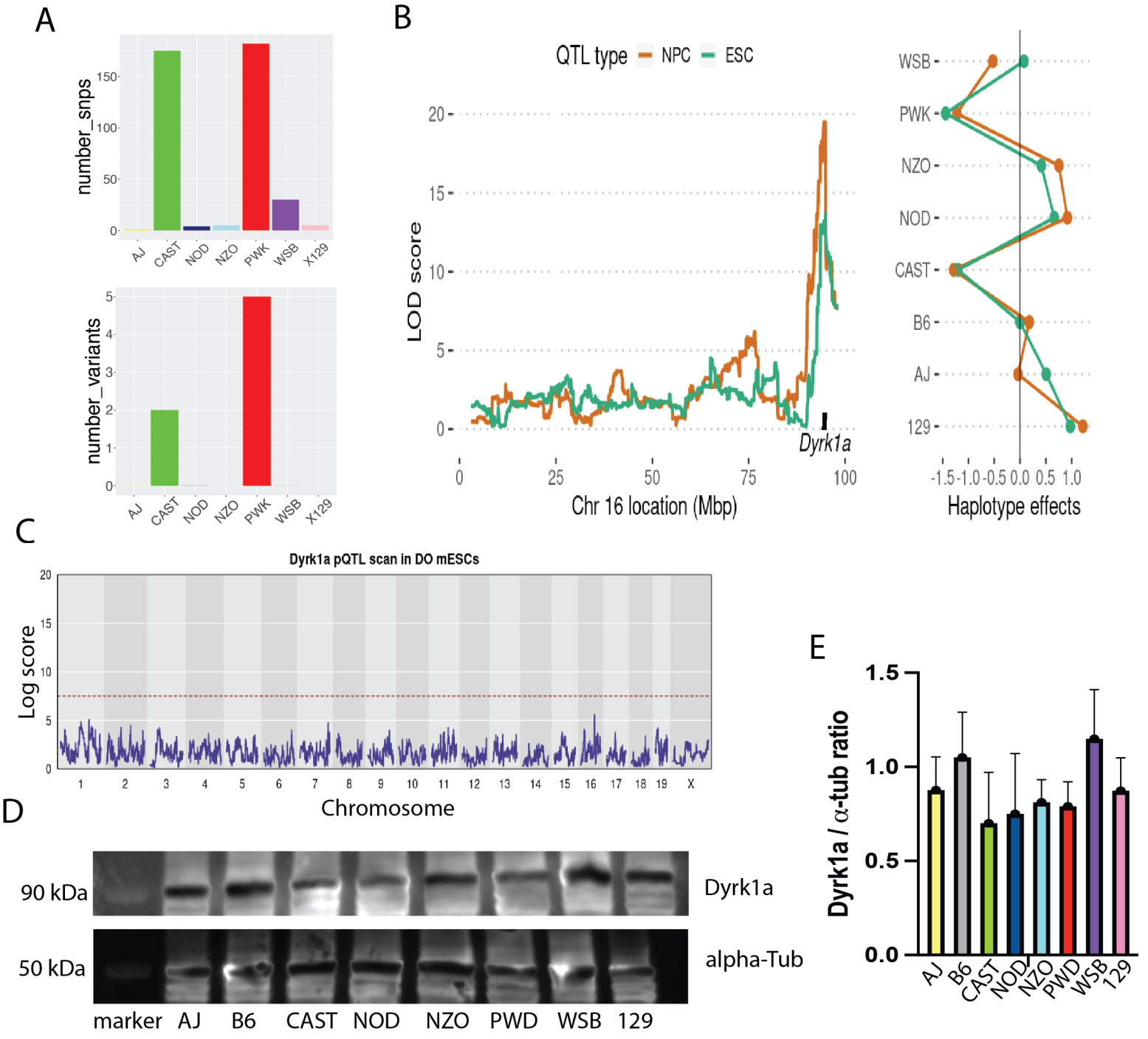
A
number_snps
150
100
50
0
AJ
CAST
NOD
NZO
PWK
WSB
X129
number_variants
5
4
3
2
1
0
B
QTL type
NPC
ESC
LOD score
20
15
10
5
0
Dyrk1a
0
25
50
75
100
Chr 16 location (Mbp)
WSB
PWK
NZO
NOD
CAST
B6
AJ
129
-1.5 -1.0 -0.5 0.0 0.5 1.0
Haplotype effects
C
Dyrk1a pQTL scan in DO mESCs
Log score
20
15
10
5
0
1
2
3
4
5
6
7
8
9
10
11
12
13
14
15
16
17
18
19
X
Chromosome
D
90 kDa
Dyrk1a
50 kDa
alpha-Tub
marker
AJ
B6
CAST
NOD
NZO
PWD
WSB
129
E
Dyrk1a / α-tub ratio
1.5
1.0
0.5
0.0
AJ
B6
CAST
NOD
NZO
PWD
WSB
129

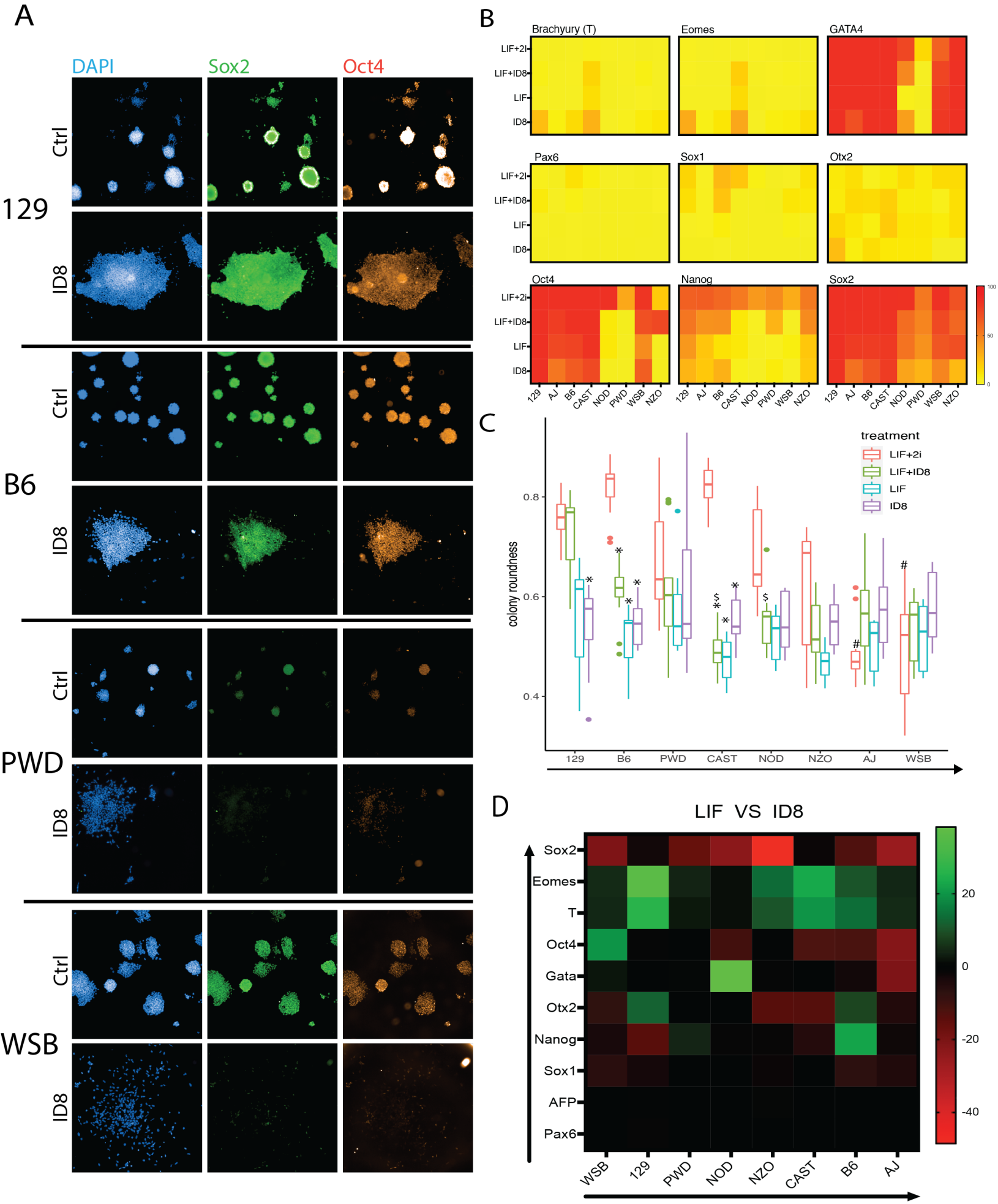
A
DAPI
Sox2
Oct4
129
Ctrl
ID8
B6
Ctrl
ID8
PWD
Ctrl
ID8
WSB
Ctrl
ID8
B
Brachyury (T)
Eomes
GATA4
Pax6
Sox1
Otx2
Oct4
Nanog
Sox2
LIF+2i
LIF+ID8
LIF
ID8
129
AJ
B6
CAST
NOD
PWD
WSB
NZO
100
50
0
C
treatment
LIF+2i
LIF+ID8
LIF
ID8
colony roundness
0.8
0.6
0.4
129
B6
PWD
CAST
NOD
NZO
AJ
WSB
D
LIF VS ID8
Sox2
Eomes
T
Oct4
Gata
Otx2
Nanog
Sox1
AFP
Pax6
WSB
129
PWD
NOD
NZO
CAST
B6
AJ
20
0
-20
-40

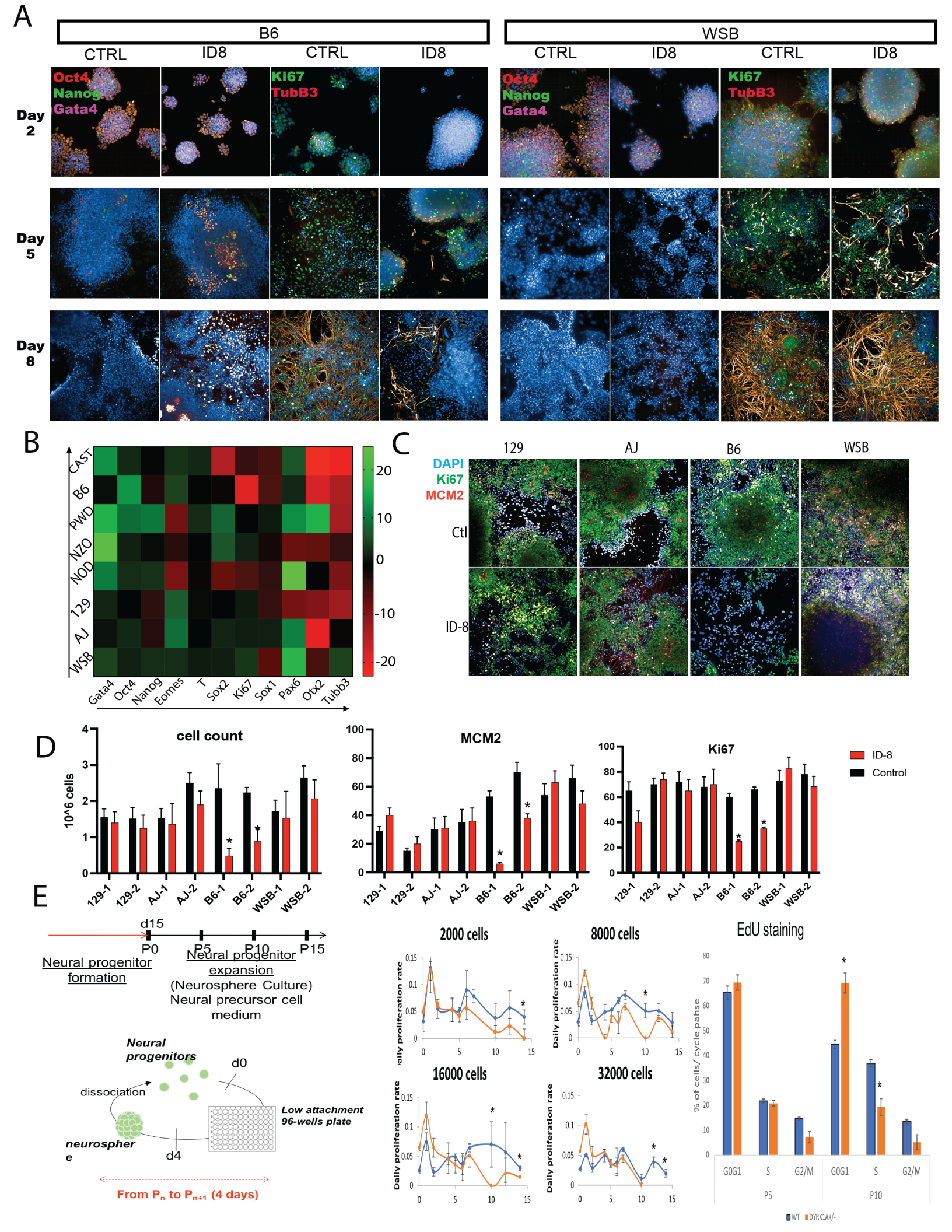
A
B6
WSB
CTRL
ID8
CTRL
ID8
CTRL
ID8
CTRL
ID8
Oct4
Nanog
Gata4
Ki67
TubB3
Day 2
Day 5
Day 8
B
CAST
B6
PWD
NZO
NOD
129
AJ
WSB
Gata4
Oct4
Nanog
Eomes
T
Sox2
Ki67
Sox1
Pax6
Otx2
Tubb3
20
10
0
-10
-20
C
129
AJ
B6
WSB
DAPI
Ki67
MCM2
Ctl
ID-8
D
cell count
10^6 cells
MCM2
Ki67
ID-8
Control
129-1
129-2
AJ-1
AJ-2
B6-1
B6-2
WSB-1
WSB-2
E
d15
P0
P5
P10
P15
Neural progenitor formation
Neural progenitor expansion
(Neurosphere Culture)
Neural precursor cell medium
Neural progenitors
d0
dissociation
neurosphere
d4
Low attachment 96-wells plate
From Pn to Pn+1 (4 days)
2000 cells
8000 cells
16000 cells
32000 cells
Daily proliferation rate
EdU staining
% of cells/ cycle pahse
G0G1
S
G2/M
P5
P10
WT
DYRK1A+/-

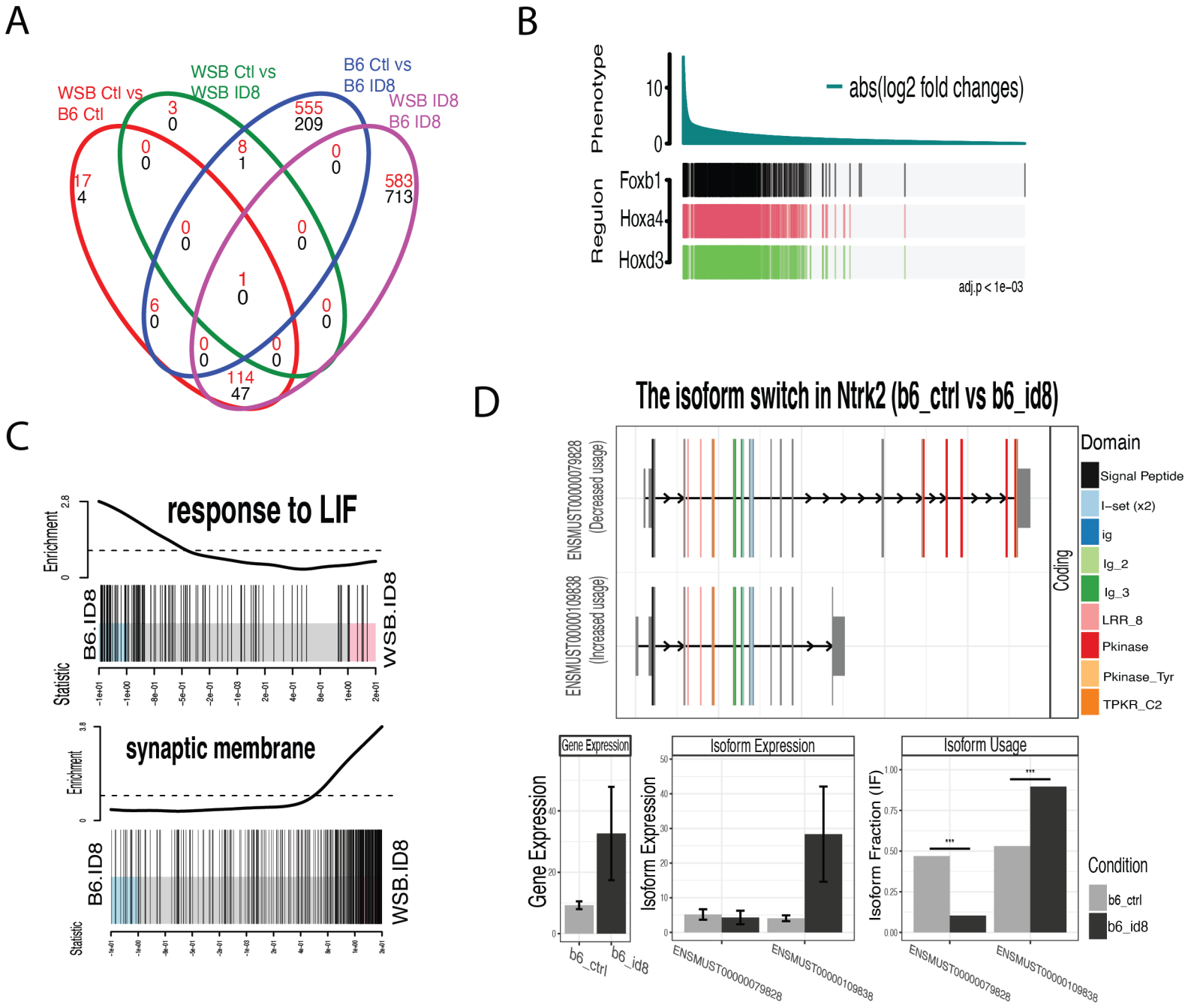
A
WSB Ctl vs B6 Ctl
WSB Ctl vs WSB ID8
B6 Ctl vs B6 ID8
WSB ID8 B6 ID8
17
4
3
0
0
0
8
1
555
209
0
0
583
713
0
0
0
0
1
0
6
0
0
0
0
0
0
0
114
47
B
Phenotype
10
0
abs(log2 fold changes)
Regulon
Foxb1
Hoxa4
Hoxd3
adj.p < 1e−03
C
response to LIF
Enrichment
2.8
0
B6.ID8
WSB.ID8
Statistic
synaptic membrane
Enrichment
3.8
0
B6.ID8
WSB.ID8
Statistic
D
The isoform switch in Ntrk2 (b6_ctrl vs b6_id8)
ENSMUST00000079828 (Decreased usage)
ENSMUST00000109838 (Increased usage)
Coding
Domain
Signal Peptide
I−set (x2)
ig
Ig_2
Ig_3
LRR_8
Pkinase
Pkinase_Tyr
TPKR_C2
Gene Expression
Gene Expression
b6_ctrl
b6_id8
Isoform Expression
Isoform Expression
ENSMUST00000079828
ENSMUST00000109838
Isoform Usage
Isoform Fraction (IF)
***
***
ENSMUST00000079828
ENSMUST00000109838
Condition
b6_ctrl
b6_id8

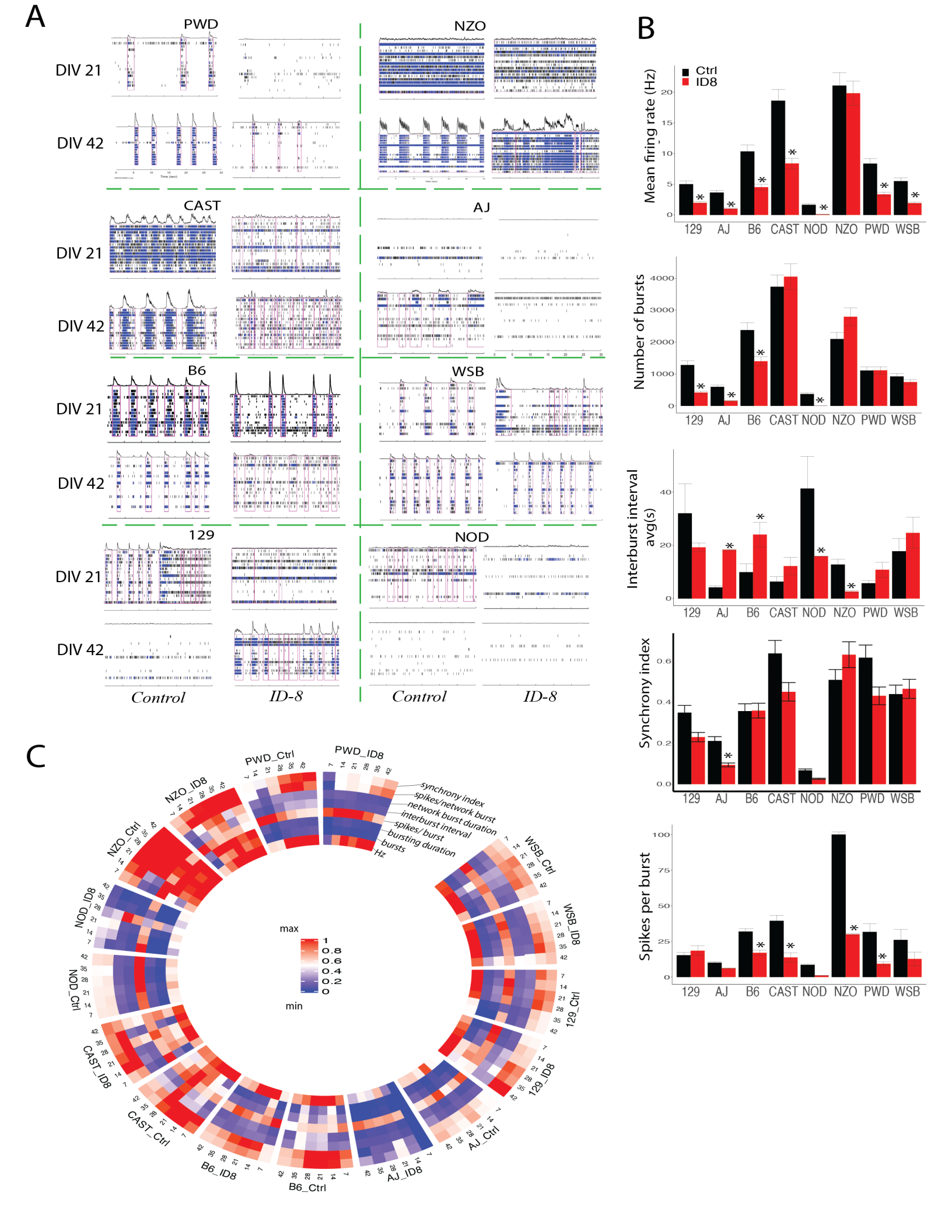
A
PWD
NZO
CAST
AJ
B6
WSB
129
NOD
DIV 21
DIV 42
Control
ID-8
B
Ctrl
ID8
Mean firing rate (Hz)
Number of bursts
Interburst interval avg(s)
Synchrony index
Spikes per burst
129
AJ
B6
CAST
NOD
NZO
PWD
WSB
C
PWD_Ctrl
PWD_ID8
NZO_ID8
NZO_Ctrl
NOD_ID8
NOD_Ctrl
CAST_ID8
CAST_Ctrl
B6_ID8
B6_Ctrl
AJ_ID8
AJ_Ctrl
129_ID8
129_Ctrl
WSB_ID8
WSB_Ctrl
synchrony index
spikes/network burst
network burst duration
interburst interval
spikes/ burst
bursting duration
bursts
Hz
max
min

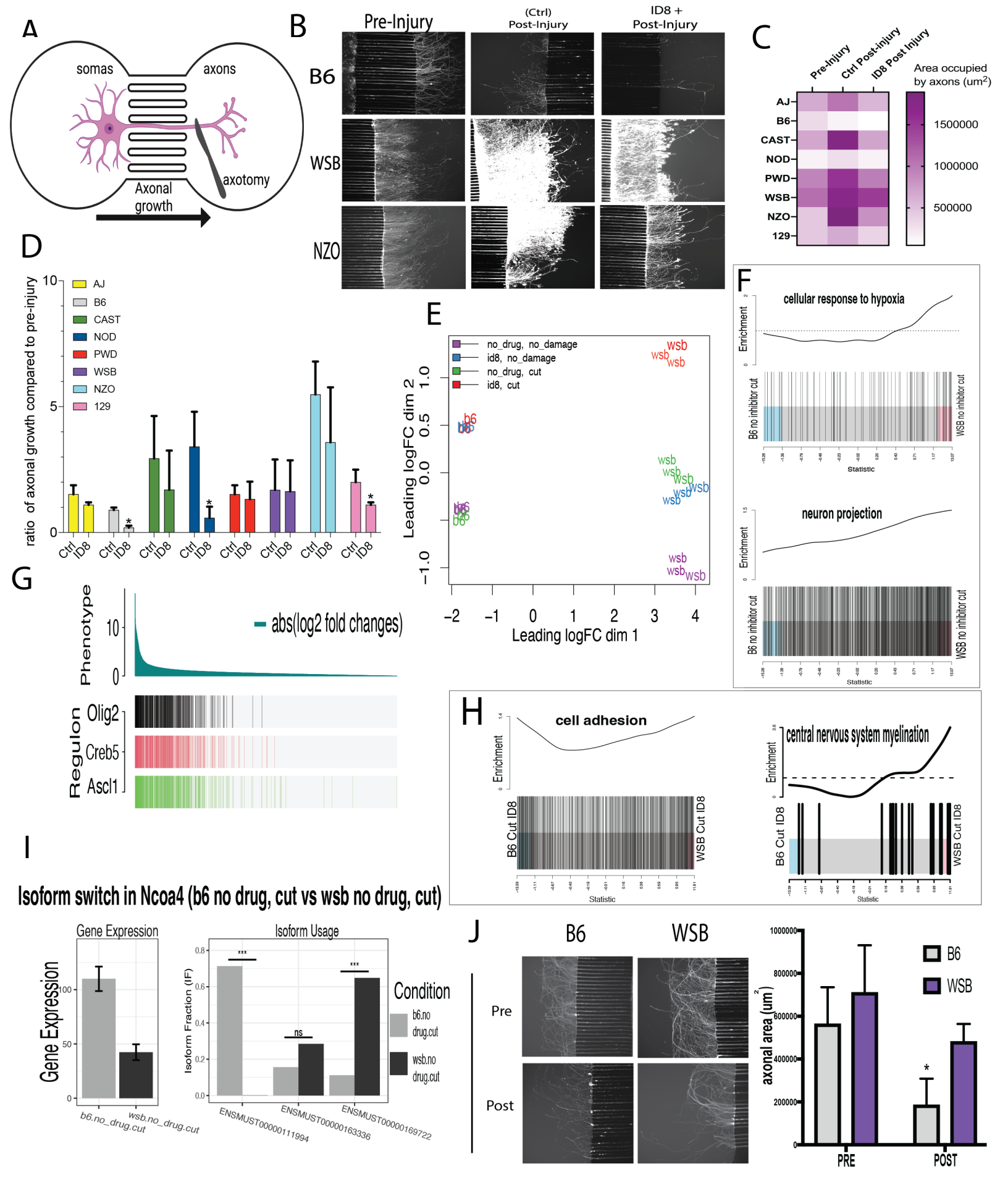
A
somas
axons
axotomy
Axonal growth
B
Pre-Injury
(Ctrl) Post-Injury
ID8 + Post-Injury
B6
WSB
NZO
C
Pre-Injury
Ctrl Post-injury
ID8 Post Injury
Area occupied by axons (um2)
AJ
B6
CAST
NOD
PWD
WSB
NZO
129
1500000
1000000
500000
D
ratio of axonal growth compared to pre-injury
AJ
B6
CAST
NOD
PWD
WSB
NZO
129
Ctrl
ID8
E
no_drug, no_damage
id8, no_damage
no_drug, cut
id8, cut
Leading logFC dim 2
Leading logFC dim 1
F
cellular response to hypoxia
neuron projection
Enrichment
B6 no inhibitor cut
WSB no inhibitor cut
Statistic
G
Phenotype
abs(log2 fold changes)
Regulon
Olig2
Creb5
Ascl1
H
cell adhesion
central nervous system myelination
Enrichment
B6 Cut ID8
WSB Cut ID8
Statistic
I
Isoform switch in Ncoa4 (b6 no drug, cut vs wsb no drug, cut)
Gene Expression
Isoform Usage
Isoform Fraction (IF)
Condition
b6.no drug.cut
wsb.no drug.cut
ns
ENSMUST00000111994
ENSMUST00000163336
ENSMUST00000169722
J
B6
WSB
Pre
Post
axonal area (um2)
PRE
POST

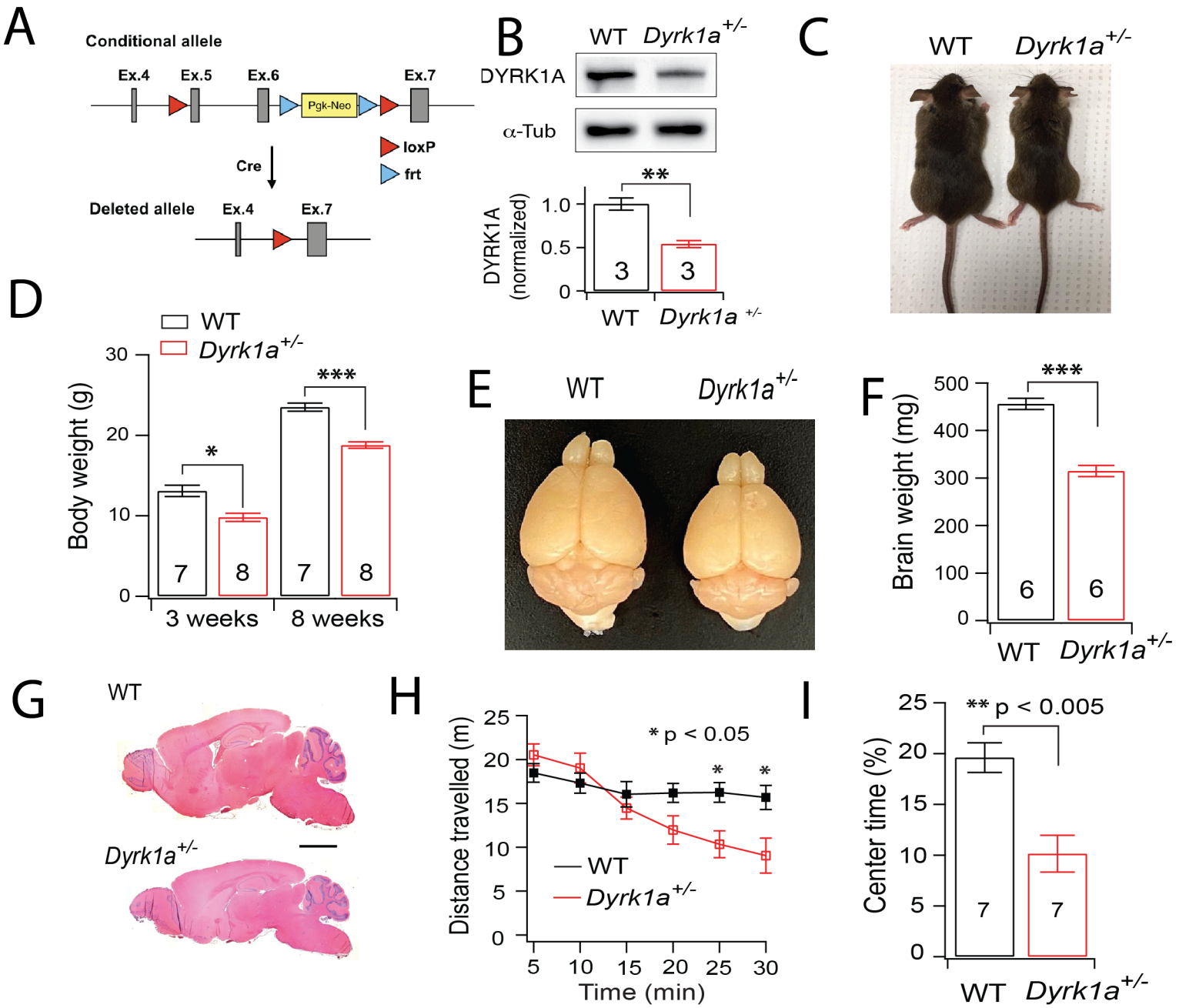
A
Conditional allele
Ex.4
Ex.5
Ex.6
Pgk-Neo
Ex.7
loxP
frt
Cre
Deleted allele
Ex.4
Ex.7
B
WT
Dyrk1a+/-
DYRK1A
α-Tub
DYRK1A (normalized)
1.0
0.5
0
**
3
3
WT
Dyrk1a +/-
C
WT
Dyrk1a+/-
D
WT
Dyrk1a+/-
Body weight (g)
30
20
10
0
*
***
7
8
7
8
3 weeks
8 weeks
E
WT
Dyrk1a+/-
F
Brain weight (mg)
500
400
300
200
100
0
***
6
6
WT
Dyrk1a+/-
G
WT
Dyrk1a+/-
H
Distance travelled (m)
25
20
15
10
5
0
* p < 0.05
*
*
WT
Dyrk1a+/-
5
10
15
20
25
30
Time (min)
I
Center time (%)
25
20
15
10
5
0
** p < 0.005
7
7
WT
Dyrk1a+/-

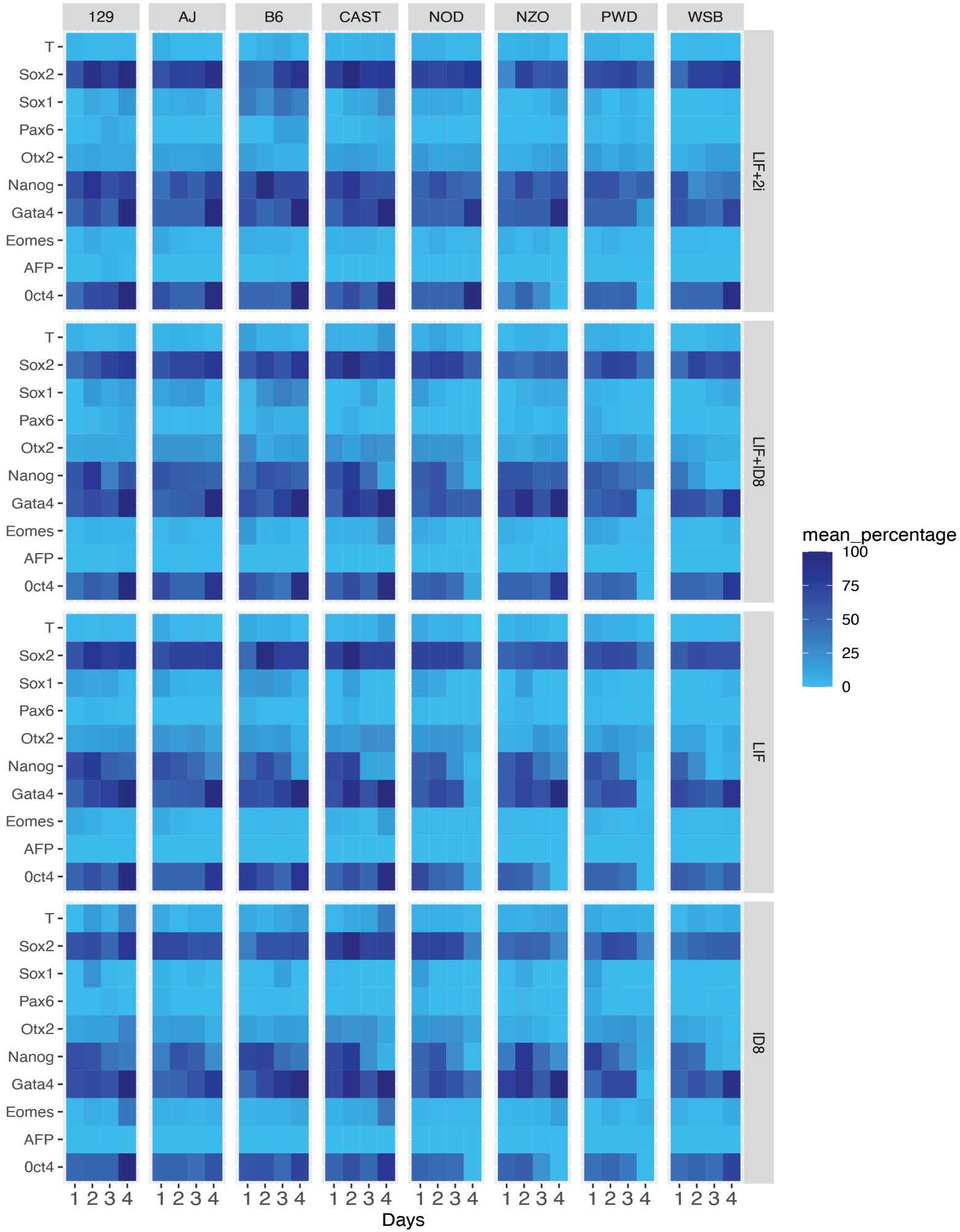

Figure S1. Heatmap of the CC foundermESC cultured in four conditions, analyzed for 4 days by IF for 10 different markers. n=4

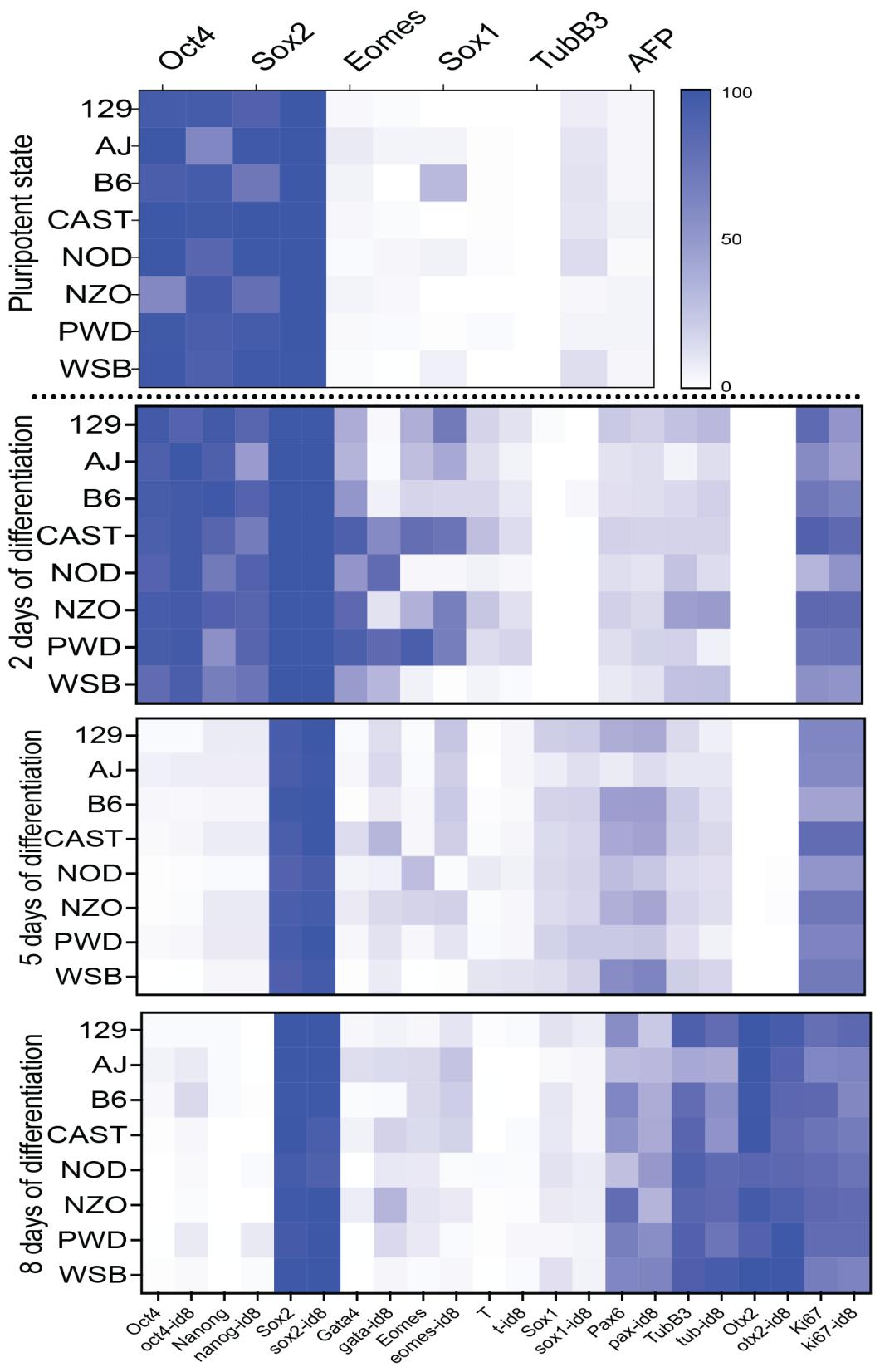

Figure S1 Heatmap for the percentage of cells positive for the analyzed markers throughout eight days of differentiation in the presence of ID-8.

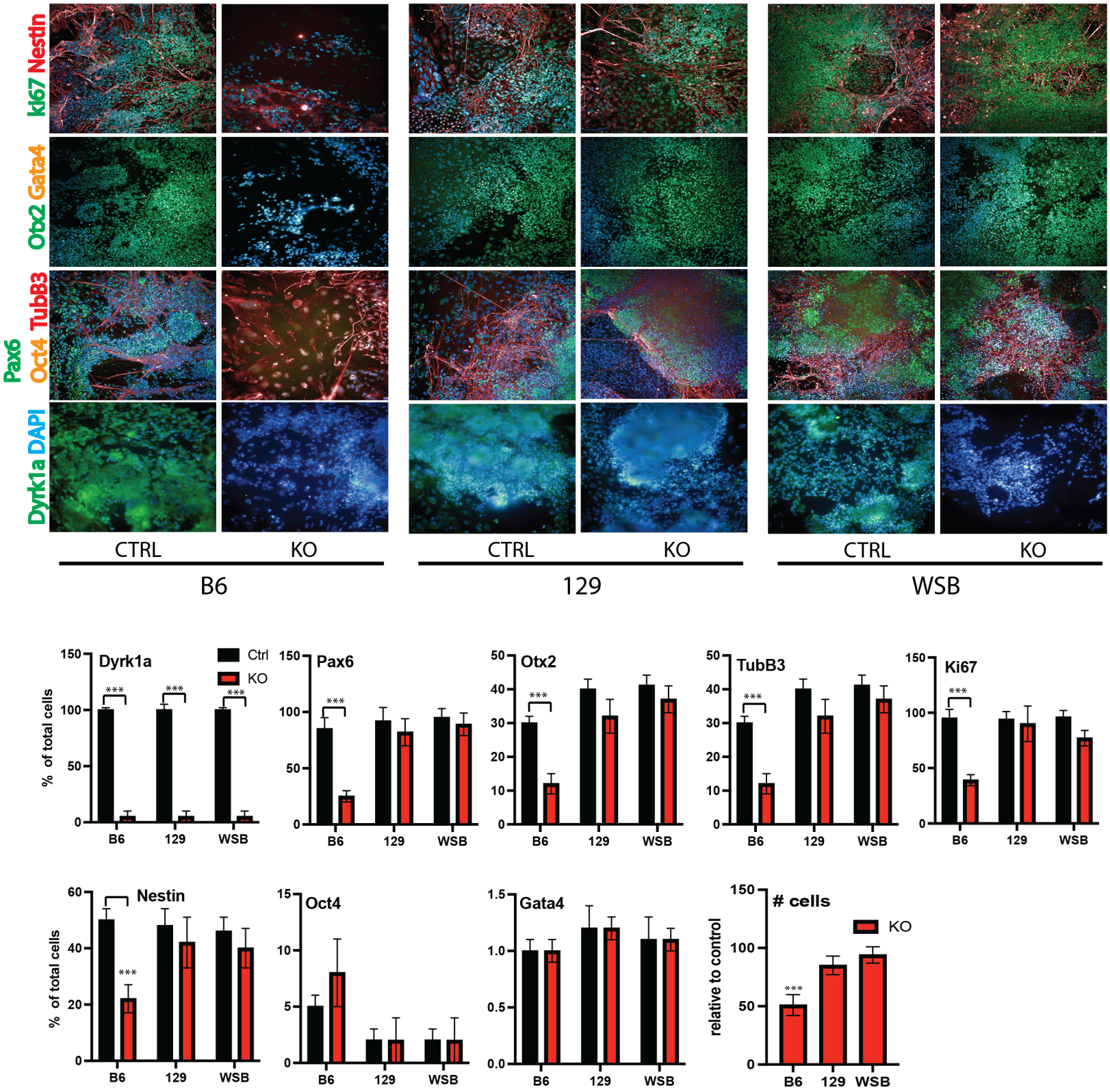

Figure S2. Neural differentiation of WT and Dyrk1a-KO mESCs. Representative images at day eight of NPC differentiation. There is a robust differentiation in all cell lines including Dyrk1a-KOs except for B6 Dyrk1a-KO. Kruskal-Wallis and Dunn's test were conducted. * = $p < 0.05$ compared to its own control n = 3 biological replicates.

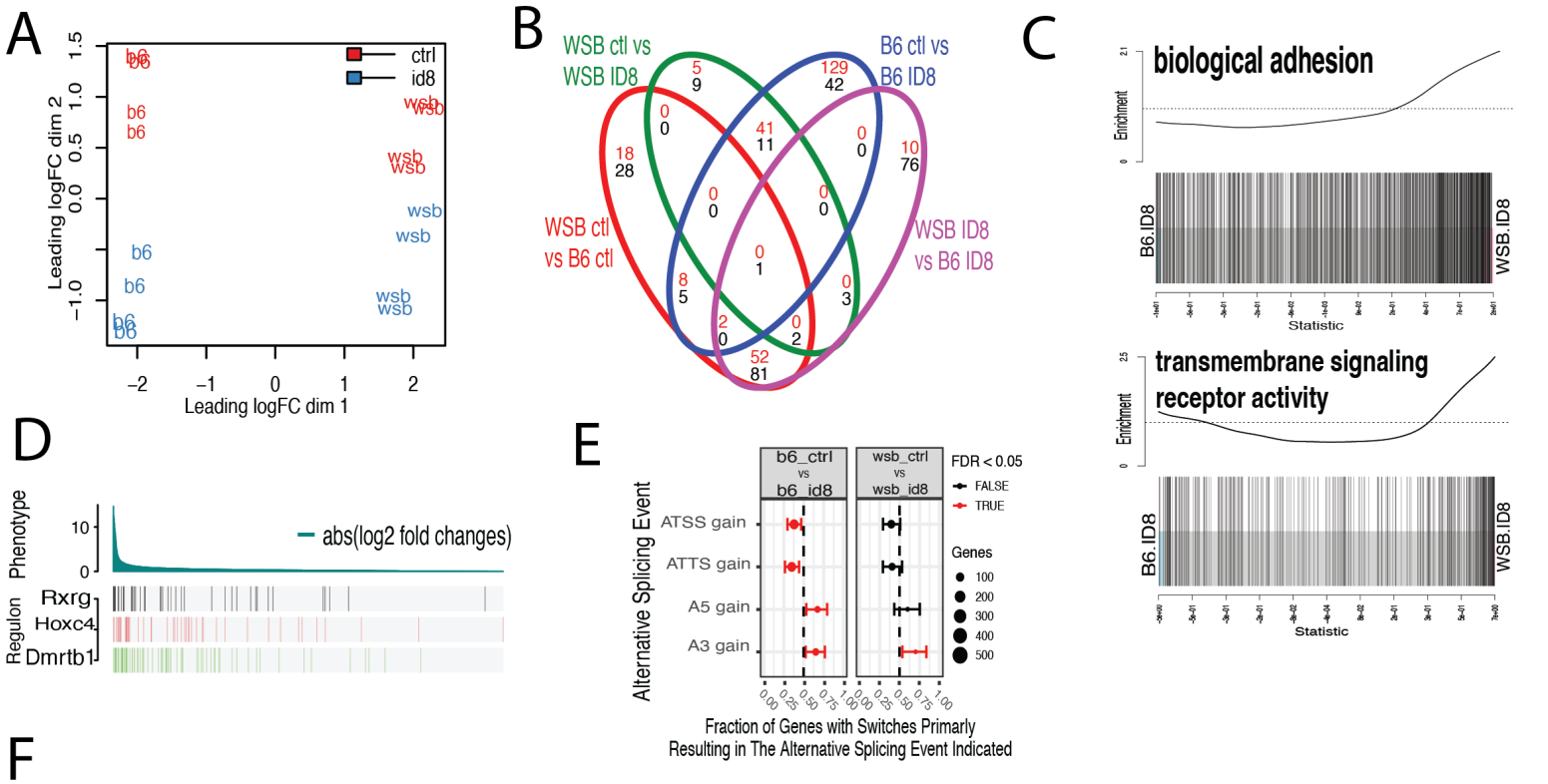

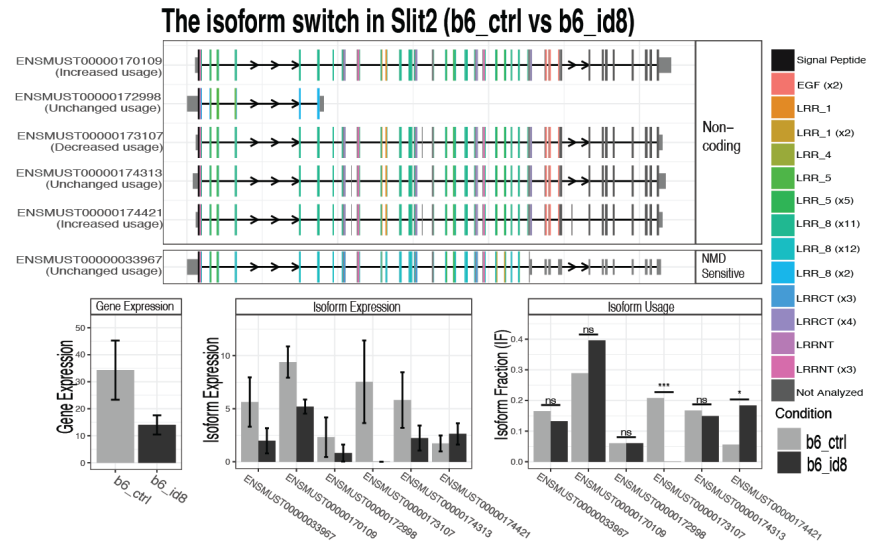

Figure S3. A) MDS plot comparing B6- and WSB-derived neurons treated or not with ID-8. It shows the distance between the groups and similarities in gene expression from RNA-seq samples. B) Venn diagram of DE genes for each set of comparisons. Number in red represents downregulated genes, black indicates upregulated genes in B6 compared to WSB. C) Exemplary barcode plots for differentially regulated gene sets. Conditions compared are indicated on both sides of the barcodes. D) RTNA for the top TFs associated with differences in ID-8 treated WSB- and B6-derived neurons. E) Alternative splicing analysis showing the change in alternative transcript start site (ATSS), alternative transcript termination site (ATTS), and alternative donor and acceptor sites (A5, A3) when B6 and WSB neurons are treated with ID8. F) Isoform switch for Slit2 in B6-derived neurons when treated with ID-8

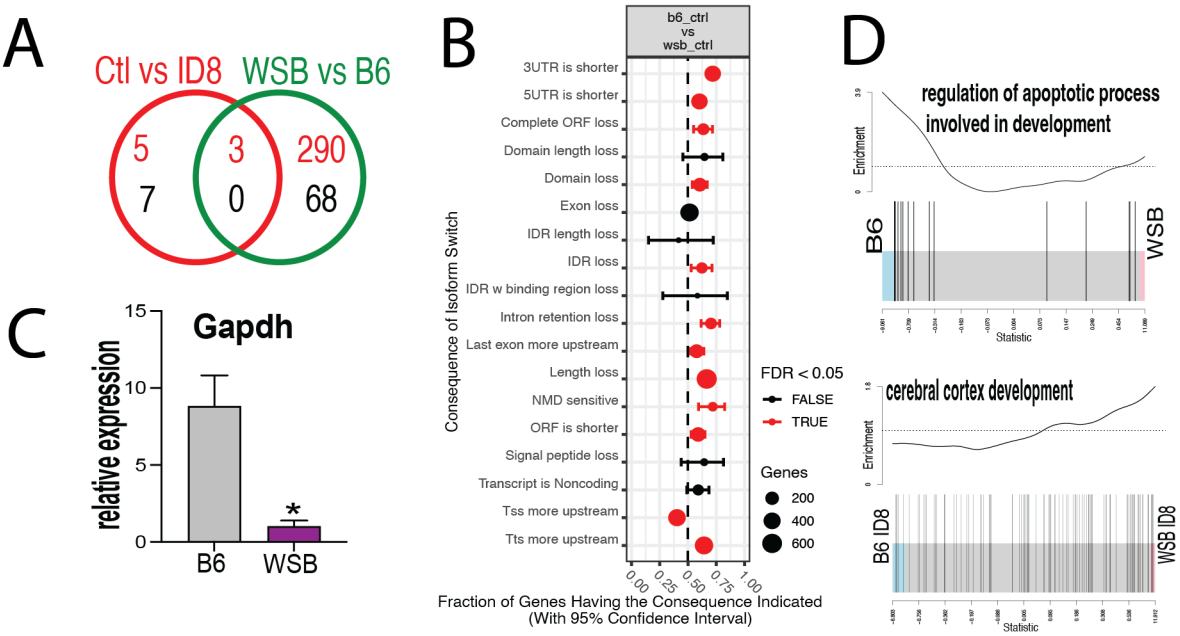

Figure S4. A) Venn diagram showing the numbers of differentially expressed genes, strain-wise and treatment-wise; B) Consequences of switch analysis between the B6 and WSB strains; C) Relative expression of Gapdh in both strains. Two-tailed T test, n = 38, *** = $p < 0.001$; D) Bar code plots showing overall differences between the two strains in control and when treated with ID-8.

CLUSTAL O(1.2.4) multiple sequence alignment

```
CAST/EiJ_MGP_CASTEiJ_P0045101
MHTGGETSACKPSSVRLAPSFSFHAAGLQMAAQMPHSHQYSDRRQPSISDQQVSALPYSD    60
129S1/SvImJ_MGP_129S1SvImJ_P0045278
MHTGGETSACKPSSVRLAPSFSFHAAGLQMAAQMPHSHQYSDRRQPSISDQQVSALPYSD    60
NZO/HlLtJ_MGP_NZOHlLtJ_P0045778
MHTGGETSACKPSSVRLAPSFSFHAAGLQMAAQMPHSHQYSDRRQPSISDQQVSALPYSD    60
NOD/ShiLtJ_MGP_NODShiLtJ_P0044977
MHTGGETSACKPSSVRLAPSFSFHAAGLQMAAQMPHSHQYSDRRQPSISDQQVSALPYSD    60
PWK/PhJ_MGP_PWKPhJ_P0044675
MHTGGETSACKPSSVRLAPSFSFHAAGLQMAAQMPHSHQYSDRRQPSISDQQVSALPYSD    60
A/J_MGP_AJ_P0045265
MHTGGETSACKPSSVRLAPSFSFHAAGLQMAAQMPHSHQYSDRRQPSISDQQVSALPYSD    60
WSB/EiJ_MGP_WSBEiJ_P0044346
MHTGGETSACKPSSVRLAPSFSFHAAGLQMAAQMPHSHQYSDRRQPSISDQQVSALPYSD    60
C57BL/6J_NP_031916.1
MHTGGETSACKPSSVRLAPSFSFHAAGLQMAAQMPHSHQYSDRRQPSISDQQVSALPYSD    60

************************************************************

CAST/EiJ_MGP_CASTEiJ_P0045101
QIQQPLTNQVMPDIVMLQRRMPQTFRDPATAPLRKLSVDLIKTYKHINEVYYAKKKRRHQ    120
129S1/SvImJ_MGP_129S1SvImJ_P0045278
QIQQPLTNQVMPDIVMLQRRMPQTFRDPATAPLRKLSVDLIKTYKHINEVYYAKKKRRHQ    120
NZO/HlLtJ_MGP_NZOHlLtJ_P0045778
QIQQPLTNQVMPDIVMLQRRMPQTFRDPATAPLRKLSVDLIKTYKHINEVYYAKKKRRHQ    120
NOD/ShiLtJ_MGP_NODShiLtJ_P0044977
QIQQPLTNQVMPDIVMLQRRMPQTFRDPATAPLRKLSVDLIKTYKHINEVYYAKKKRRHQ    120
PWK/PhJ_MGP_PWKPhJ_P0044675
QIQQPLTNQVMPDIVMLQRRMPQTFRDPATAPLRKLSVDLIKTYKHINEVYYAKKKRRHQ    120
A/J_MGP_AJ_P0045265
QIQQPLTNQVMPDIVMLQRRMPQTFRDPATAPLRKLSVDLIKTYKHINEVYYAKKKRRHQ    120
WSB/EiJ_MGP_WSBEiJ_P0044346
QIQQPLTNQVMPDIVMLQRRMPQTFRDPATAPLRKLSVDLIKTYKHINEVYYAKKKRRHQ    120
C57BL/6J_NP_031916.1
QIQQPLTNQVMPDIVMLQRRMPQTFRDPATAPLRKLSVDLIKTYKHINEVYYAKKKRRHQ    120

************************************************************

CAST/EiJ_MGP_CASTEiJ_P0045101
QGQGDDSSHKKERKVYNDGYDDDNYDYIVKNGEKWMDRYEIDSLIGKGSFGQVVKAYDRV    180
129S1/SvImJ_MGP_129S1SvImJ_P0045278
QGQGDDSSHKKERKVYNDGYDDDNYDYIVKNGEKWMDRYEIDSLIGKGSFGQVVKAYDRV    180
NZO/HlLtJ_MGP_NZOHlLtJ_P0045778
QGQGDDSSHKKERKVYNDGYDDDNYDYIVKNGEKWMDRYEIDSLIGKGSFGQVVKAYDRV    180
NOD/ShiLtJ_MGP_NODShiLtJ_P0044977
QGQGDDSSHKKERKVYNDGYDDDNYDYIVKNGEKWMDRYEIDSLIGKGSFGQVVKAYDRV    180
PWK/PhJ_MGP_PWKPhJ_P0044675
QGQGDDSSHKKERKVYNDGYDDDNYDYIVKNGEKWMDRYEIDSLIGKGSFGQVVKAYDRV    180
A/J_MGP_AJ_P0045265
QGQGDDSSHKKERKVYNDGYDDDNYDYIVKNGEKWMDRYEIDSLIGKGSFGQVVKAYDRV    180
WSB/EiJ_MGP_WSBEiJ_P0044346
QGQGDDSSHKKERKVYNDGYDDDNYDYIVKNGEKWMDRYEIDSLIGKGSFGQVVKAYDRV    180
C57BL/6J_NP_031916.1
QGQGDDSSHKKERKVYNDGYDDDNYDYIVKNGEKWMDRYEIDSLIGKGSFGQVVKAYDRV    180

************************************************************

CAST/EiJ_MGP_CASTEiJ_P0045101
EQEWVAIKIIKNKKAFLNQAQIEVRLLELMNKHDTEMKYYIVHLKRHFMFRNHLCLVFEM    240
129S1/SvImJ_MGP_129S1SvImJ_P0045278
EQEWVAIKIIKNKKAFLNQAQIEVRLLELMNKHDTEMKYYIVHLKRHFMFRNHLCLVFEM    240
NZO/HlLtJ_MGP_NZOHlLtJ_P0045778
EQEWVAIKIIKNKKAFLNQAQIEVRLLELMNKHDTEMKYYIVHLKRHFMFRNHLCLVFEM    240
NOD/ShiLtJ_MGP_NODShiLtJ_P0044977
EQEWVAIKIIKNKKAFLNQAQIEVRLLELMNKHDTEMKYYIVHLKRHFMFRNHLCLVFEM    240
PWK/PhJ_MGP_PWKPhJ_P0044675
EQEWVAIKIIKNKKAFLNQAQIEVRLLELMNKHDTEMKYYIVHLKRHFMFRNHLCLVFEM    240
A/J_MGP_AJ_P0045265
EQEWVAIKIIKNKKAFLNQAQIEVRLLELMNKHDTEMKYYIVHLKRHFMFRNHLCLVFEM    240
WSB/EiJ_MGP_WSBEiJ_P0044346
EQEWVAIKIIKNKKAFLNQAQIEVRLLELMNKHDTEMKYYIVHLKRHFMFRNHLCLVFEM    240
C57BL/6J_NP_031916.1
EQEWVAIKIIKNKKAFLNQAQIEVRLLELMNKHDTEMKYYIVHLKRHFMFRNHLCLVFEM    240

************************************************************

CAST/EiJ_MGP_CASTEiJ_P0045101
```

```
LSYNLYDLLRNTNFRGVSLNLTRKFAQQMCTALLFLATPELSIIHCDLKPENILLCNPKR    300
129S1/SvImJ_MGP_129S1SvImJ_P0045278
LSYNLYDLLRNTNFRGVSLNLTRKFAQQMCTALLFLATPELSIIHCDLKPENILLCNPKR    300
NZO/HlLtJ_MGP_NZOHlLtJ_P0045778
LSYNLYDLLRNTNFRGVSLNLTRKFAQQMCTALLFLATPELSIIHCDLKPENILLCNPKR    300
NOD/ShiLtJ_MGP_NODShiLtJ_P0044977
LSYNLYDLLRNTNFRGVSLNLTRKFAQQMCTALLFLATPELSIIHCDLKPENILLCNPKR    300
PWK/PhJ_MGP_PWKPhJ_P0044675
LSYNLYDLLRNTNFRGVSLNLTRKFAQQMCTALLFLATPELSIIHCDLKPENILLCNPKR    300
A/J_MGP_AJ_P0045265
LSYNLYDLLRNTNFRGVSLNLTRKFAQQMCTALLFLATPELSIIHCDLKPENILLCNPKR    300
WSB/EiJ_MGP_WSBEiJ_P0044346
LSYNLYDLLRNTNFRGVSLNLTRKFAQQMCTALLFLATPELSIIHCDLKPENILLCNPKR    300
C57BL/6J_NP_031916.1
LSYNLYDLLRNTNFRGVSLNLTRKFAQQMCTALLFLATPELSIIHCDLKPENILLCNPKR    300

************************************************************

CAST/EiJ_MGP_CASTEiJ_P0045101
SAIKIVDFGSSCQLGQRIYQYIQSRFYRSPEVLLGMPYDLAIDMWSLGCILVEMHTGEPL    360
129S1/SvImJ_MGP_129S1SvImJ_P0045278
SAIKIVDFGSSCQLGQRIYQYIQSRFYRSPEVLLGMPYDLAIDMWSLGCILVEMHTGEPL    360
NZO/HlLtJ_MGP_NZOHlLtJ_P0045778
SAIKIVDFGSSCQLGQRIYQYIQSRFYRSPEVLLGMPYDLAIDMWSLGCILVEMHTGEPL    360
NOD/ShiLtJ_MGP_NODShiLtJ_P0044977
SAIKIVDFGSSCQLGQRIYQYIQSRFYRSPEVLLGMPYDLAIDMWSLGCILVEMHTGEPL    360
PWK/PhJ_MGP_PWKPhJ_P0044675
SAIKIVDFGSSCQLGQRIYQYIQSRFYRSPEVLLGMPYDLAIDMWSLGCILVEMHTGEPL    360
A/J_MGP_AJ_P0045265
SAIKIVDFGSSCQLGQRIYQYIQSRFYRSPEVLLGMPYDLAIDMWSLGCILVEMHTGEPL    360
WSB/EiJ_MGP_WSBEiJ_P0044346
SAIKIVDFGSSCQLGQRIYQYIQSRFYRSPEVLLGMPYDLAIDMWSLGCILVEMHTGEPL    360
C57BL/6J_NP_031916.1
SAIKIVDFGSSCQLGQRIYQYIQSRFYRSPEVLLGMPYDLAIDMWSLGCILVEMHTGEPL    360

************************************************************

CAST/EiJ_MGP_CASTEiJ_P0045101
FSGANEVDQMNKIVEVLGIPPAHILDQAPKARKFFEKLPDGTWSLKKTKDGKREYKPPGT    420
129S1/SvImJ_MGP_129S1SvImJ_P0045278
FSGANEVDQMNKIVEVLGIPPAHILDQAPKARKFFEKLPDGTWSLKKTKDGKREYKPPGT    420
NZO/HlLtJ_MGP_NZOHlLtJ_P0045778
FSGANEVDQMNKIVEVLGIPPAHILDQAPKARKFFEKLPDGTWSLKKTKDGKREYKPPGT    420
NOD/ShiLtJ_MGP_NODShiLtJ_P0044977
FSGANEVDQMNKIVEVLGIPPAHILDQAPKARKFFEKLPDGTWSLKKTKDGKREYKPPGT    420
PWK/PhJ_MGP_PWKPhJ_P0044675
FSGANEVDQMNKIVEVLGIPPAHILDQAPKARKFFEKLPDGTWSLKKTKDGKREYKPPGT    420
A/J_MGP_AJ_P0045265
FSGANEVDQMNKIVEVLGIPPAHILDQAPKARKFFEKLPDGTWSLKKTKDGKREYKPPGT    420
WSB/EiJ_MGP_WSBEiJ_P0044346
FSGANEVDQMNKIVEVLGIPPAHILDQAPKARKFFEKLPDGTWSLKKTKDGKREYKPPGT    420
C57BL/6J_NP_031916.1
FSGANEVDQMNKIVEVLGIPPAHILDQAPKARKFFEKLPDGTWSLKKTKDGKREYKPPGT    420

************************************************************

CAST/EiJ_MGP_CASTEiJ_P0045101
RKLHNILGVETGGPGGRRAGESGHTVADYLKFKDLILRMLDYDPKTRIQPYYALQHSFFK    480
129S1/SvImJ_MGP_129S1SvImJ_P0045278
RKLHNILGVETGGPGGRRAGESGHTVADYLKFKDLILRMLDYDPKTRIQPYYALQHSFFK    480
NZO/HlLtJ_MGP_NZOHlLtJ_P0045778
RKLHNILGVETGGPGGRRAGESGHTVADYLKFKDLILRMLDYDPKTRIQPYYALQHSFFK    480
NOD/ShiLtJ_MGP_NODShiLtJ_P0044977
RKLHNILGVETGGPGGRRAGESGHTVADYLKFKDLILRMLDYDPKTRIQPYYALQHSFFK    480
PWK/PhJ_MGP_PWKPhJ_P0044675
RKLHNILGVETGGPGGRRAGESGHTVADYLKFKDLILRMLDYDPKTRIQPYYALQHSFFK    480
A/J_MGP_AJ_P0045265
RKLHNILGVETGGPGGRRAGESGHTVADYLKFKDLILRMLDYDPKTRIQPYYALQHSFFK    480
WSB/EiJ_MGP_WSBEiJ_P0044346
RKLHNILGVETGGPGGRRAGESGHTVADYLKFKDLILRMLDYDPKTRIQPYYALQHSFFK    480
C57BL/6J_NP_031916.1
RKLHNILGVETGGPGGRRAGESGHTVADYLKFKDLILRMLDYDPKTRIQPYYALQHSFFK    480

************************************************************

CAST/EiJ_MGP_CASTEiJ_P0045101
KTADEGTNTSNSVSTSPAMEQSQSSGTTSSTSSSSGGSSGTSNSGRARSDPTHQHRHSGG    540
129S1/SvImJ_MGP_129S1SvImJ_P0045278
KTADEGTNTSNSVSTSPAMEQSQSSGTTSSTSSSSGGSSGTSNSGRARSDPTHQHRHSGG    540
NZO/HlLtJ_MGP_NZOHlLtJ_P0045778
KTADEGTNTSNSVSTSPAMEQSQSSGTTSSTSSSSGGSSGTSNSGRARSDPTHQHRHSGG    540
```

```
NOD/ShiLtJ_MGP_NODShiLtJ_P0044977
KTADEGTNTSNSVSTSPAMEQSQSSGTTSSTSSSSGGSSGTSNSGRARSDPTHQHRHSGG    540
PWK/PhJ_MGP_PWKPhJ_P0044675
KTADEGTNTSNSVSTSPAMEQSQSSGTTSSTSSSSGGSSGTSNSGRARSDPTHQHRHSGG    540
A/J_MGP_AJ_P0045265
KTADEGTNTSNSVSTSPAMEQSQSSGTTSSTSSSSGGSSGTSNSGRARSDPTHQHRHSGG    540
WSB/EiJ_MGP_WSBEiJ_P0044346
KTADEGTNTSNSVSTSPAMEQSQSSGTTSSTSSSSGGSSGTSNSGRARSDPTHQHRHSGG    540
C57BL/6J_NP_031916.1
KTADEGTNTSNSVSTSPAMEQSQSSGTTSSTSSSSGGSSGTSNSGRARSDPTHQHRHSGG    540

************************************************************

CAST/EiJ_MGP_CASTEiJ_P0045101
HFAAAVQAMDCETHSPQVRQQFPAPLGWSGTEAPTQVTVETHPVQETTFHVAPQQNALHH    600
129S1/SvImJ_MGP_129S1SvImJ_P0045278
HFAAAVQAMDCETHSPQVRQQFPAPLGWSGTEAPTQVTVETHPVQETTFHVAPQQNALHH    600
NZO/HlLtJ_MGP_NZOHlLtJ_P0045778
HFAAAVQAMDCETHSPQVRQQFPAPLGWSGTEAPTQVTVETHPVQETTFHVAPQQNALHH    600
NOD/ShiLtJ_MGP_NODShiLtJ_P0044977
HFAAAVQAMDCETHSPQVRQQFPAPLGWSGTEAPTQVTVETHPVQETTFHVAPQQNALHH    600
PWK/PhJ_MGP_PWKPhJ_P0044675
HFAAAVQAMDCETHSPQVRQQFPAPLGWSGTEAPTQVTVETHPVQETTFHVAPQQNALHH    600
A/J_MGP_AJ_P0045265
HFAAAVQAMDCETHSPQVRQQFPAPLGWSGTEAPTQVTVETHPVQETTFHVAPQQNALHH    600
WSB/EiJ_MGP_WSBEiJ_P0044346
HFAAAVQAMDCETHSPQVRQQFPAPLGWSGTEAPTQVTVETHPVQETTFHVAPQQNALHH    600
C57BL/6J_NP_031916.1
HFAAAVQAMDCETHSPQVRQQFPAPLGWSGTEAPTQVTVETHPVQETTFHVAPQQNALHH    600

************************************************************

CAST/EiJ_MGP_CASTEiJ_P0045101
HHGNSSHHHHHHHHHHHHHHGQQALGNRTRPRVYNSPTNSSSTQDSMEVGHSHHSMTSLSS    660
129S1/SvImJ_MGP_129S1SvImJ_P0045278
HHGNSSHHHHHHHHHHHHHHGQQALGNRTRPRVYNSPTNSSSTQDSMEVGHSHHSMTSLSS    660
NZO/HlLtJ_MGP_NZOHlLtJ_P0045778
HHGNSSHHHHHHHHHHHHHHGQQALGNRTRPRVYNSPTNSSSTQDSMEVGHSHHSMTSLSS    660
NOD/ShiLtJ_MGP_NODShiLtJ_P0044977
HHGNSSHHHHHHHHHHHHHHGQQALGNRTRPRVYNSPTNSSSTQDSMEVGHSHHSMTSLSS    660
PWK/PhJ_MGP_PWKPhJ_P0044675
HHGNSSHHHHHHHHHHHHHHGQQALGNRTRPRVYNSPTNSSSTQDSMEVGHSHHSMTSLSS    660
A/J_MGP_AJ_P0045265
HHGNSSHHHHHHHHHHHHHHGQQALGNRTRPRVYNSPTNSSSTQDSMEVGHSHHSMTSLSS    660
WSB/EiJ_MGP_WSBEiJ_P0044346
HHGNSSHHHHHHHHHHHHHHGQQALGNRTRPRVYNSPTNSSSTQDSMEVGHSHHSMTSLSS    660
C57BL/6J_NP_031916.1
HHGNSSHHHHHHHHHHHHHHGQQALGNRTRPRVYNSPTNSSSTQDSMEVGHSHHSMTSLSS    660

************************************************************

CAST/EiJ_MGP_CASTEiJ_P0045101
STTSSSTSSSSTGNQGNQAYQNRPVAANTLDFGQNGAMDVNLTVYSNPRQETGIAGHPTY    720
129S1/SvImJ_MGP_129S1SvImJ_P0045278
STTSSSTSSSSTGNQGNQAYQNRPVAANTLDFGQNGAMDVNLTVYSNPRQETGIAGHPTY    720
NZO/HlLtJ_MGP_NZOHlLtJ_P0045778
STTSSSTSSSSTGNQGNQAYQNRPVAANTLDFGQNGAMDVNLTVYSNPRQETGIAGHPTY    720
NOD/ShiLtJ_MGP_NODShiLtJ_P0044977
STTSSSTSSSSTGNQGNQAYQNRPVAANTLDFGQNGAMDVNLTVYSNPRQETGIAGHPTY    720
PWK/PhJ_MGP_PWKPhJ_P0044675
STTSSSTSSSSTGNQGNQAYQNRPVAANTLDFGQNGAMDVNLTVYSNPRQETGIAGHPTY    720
A/J_MGP_AJ_P0045265
STTSSSTSSSSTGNQGNQAYQNRPVAANTLDFGQNGAMDVNLTVYSNPRQETGIAGHPTY    720
WSB/EiJ_MGP_WSBEiJ_P0044346
STTSSSTSSSSTGNQGNQAYQNRPVAANTLDFGQNGAMDVNLTVYSNPRQETGIAGHPTY    720
C57BL/6J_NP_031916.1
STTSSSTSSSSTGNQGNQAYQNRPVAANTLDFGQNGAMDVNLTVYSNPRQETGIAGHPTY    720

************************************************************

CAST/EiJ_MGP_CASTEiJ_P0045101            QFSANTGPAHYMTEGHLAMRQGADREESPMTGVCVQQSPVASS    763
129S1/SvImJ_MGP_129S1SvImJ_P0045278      QFSANTGPAHYMTEGHLAMRQGADREESPMTGVCVQQSPVASS    763
NZO/HlLtJ_MGP_NZOHlLtJ_P0045778          QFSANTGPAHYMTEGHLAMRQGADREESPMTGVCVQQSPVASS    763
NOD/ShiLtJ_MGP_NODShiLtJ_P0044977        QFSANTGPAHYMTEGHLAMRQGADREESPMTGVCVQQSPVASS    763
PWK/PhJ_MGP_PWKPhJ_P0044675              QFSANTGPAHYMTEGHLAMRQGADREESPMTGVCVQQSPVASS    763
A/J_MGP_AJ_P0045265                      QFSANTGPAHYMTEGHLAMRQGADREESPMTGVCVQQSPVASS    763
WSB/EiJ_MGP_WSBEiJ_P0044346              QFSANTGPAHYMTEGHLAMRQGADREESPMTGVCVQQSPVASS    763
C57BL/6J_NP_031916.1                     QFSANTGPAHYMTEGHLAMRQGADREESPMTGVCVQQSPVASS    763
                                         ******************************************
```

Document S1. Sequence alignment of Dyrk1a gene from the eight CC mESC founders found no differences in the protein sequence.